NASA CR-134718

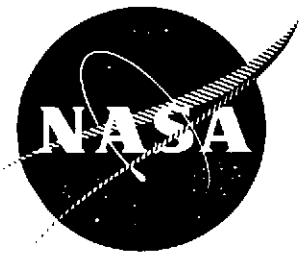

PARTICLE FLOW WITHIN A TRANSONIC COMPRESSOR ROTOR PASSAGE WITH APPLICATION TO LASER-DOPPLER VELOCIMETRY

by Barry R. Maxwell

BUCKNELL UNIVERSITY

Lewisburg, Pennsylvania 17837

prepared for

NATIONAL AERONAUTICS AND SPACE ADMINISTRATION

NASA Lewis Research Center

NASA GRANT NGR-39-027-003

1. Report No.	2. Government Accession No.	3. Recipient's Catalog No.
NASA CR-134718		

4. Title and Subtitle	5. Report Date
PARTICLE FLOW WITHIN A TRANSONIC COMPRESSOR ROTOR PASSAGE WITH APPLICATION TO LASER-DOPPLER VELOCIMETRY	February 1975
	6. Performing Organization Code

7. Author(s)	8. Performing Organization Report No.
Barry R. Maxwell	
	10. Work Unit No.

9. Performing Organization Name and Address	11. Contract or Grant No.
Bucknell University Lewisburg, Pa. 17837	NGR-39-027-003
	13. Type of Report and Period Covered
12. Sponsoring Agency Name and Address	Contractor Report
National Aeronautics and Space Administration Washington, DC 20546	14. Sponsoring Agency Code

15. Supplementary Notes

Project Manager, Richard G. Seasholtz, Instrument Development Applications Office
NASA-Lewis Reasearch Center, Cleveland, OH 44135

16. Abstract

A theoretical analysis was conducted of the dynamic behavior of micron size particles moving in the three-dimensional flow field of a rotating transonic axial-flow air compressor rotor. The particle velocity lag and angular deviation relative to the gas were determined as functions of particle diameter, mass density and radial position. Particle size and density were varied over ranges selected to correspond to typical laser-Doppler velocimeter (LDV) flow field mapping applications. It was found that the particles move essentially on gas stream surfaces and that particle tracking is relatively insensitive to the rotor radial coordinate. Velocity lag and angular deviation increased whenever particle size or mass density increased, and particle tracking was more sensitive to a change in particle diameter than to a corresponding change in mass density. Results indicated that velocity and angular deviations generally less than 1 percent and 1 degree could be achieved with 1 gm/cc tracer particles with diameters of 1 micron or less.

17. Key Words (Suggested by Author(s))	18. Distribution Statement
Laser-Doppler Velocimetry Particle Flow Turbomachinery	Unclassified-unlimited

19. Security Classif. (of this report)	20. Security Classif. (of this page)	21. No. of Pages	22. Price*
Unclassified	Unclassified		$3.00

*For sale by the National Technical Information Service, Springfield, Virginia 22151

TABLE OF CONTENTS

LIST OF FIGURES

PARTICLE FLOW WITHIN A TRANSONIC COMPRESSOR ROTOR PASSAGE WITH APPLICATION TO LASER-DOPPLER VELOCIMETRY

by Barry R. Maxwell

Bucknell University

SUMMARY

A theoretical analysis was conducted of the dynamic behavior of micron size particles moving in the three-dimensional flow field of a rotating transonic axial-flow air compressor rotor. The particle velocity lag and angular deviation relative to the gas were determined as functions of particle diameter, mass density, and radial position. Particle size and density were varied over ranges selected to correspond to typical laser-Doppler velocimeter (LDV) flow field mapping applications. It was found that the particles move essentially on gas stream surfaces and that particle tracking is relatively insensitive to the rotor radial coordinate. Velocity lag and angular deviation increased whenever particle size or mass density increased, and particle tracking was more sensitive to a change in particle diameter than to a corresponding change in mass density. Results indicated that velocity and angular deviations generally less than 1 percent and 1 degree could be achieved with 1 gm/cc tracer particles with diameters of 1 micron or less.

INTRODUCTION

Laser-Doppler Velocimetry (LDV) is a noncontact optical technique for determining the velocity of flowing fluids by measuring the velocity of tracer particles entrained in the fluid rather than by measuring the velocity of the fluid itself. The LDV technique is of considerable importance in gas dynamic measurements because it is unnecessary to introduce any hardware into the flow system. Because of the absence of a physical probe the LDV technique is ideally suited to measuring gas velocities in the flow passages between rotor and stator blades of turbomachines. Development of noncontact velocimetry techniques in turbomachinery will provide data currently required to extend and improve design methods, blade performance and efficiency of components used in advanced airbreathing engines. It is for this reason that the LDV technique is beginning to find application in the aircraft turbomachinery field (ref. 1,2).

The laser-Doppler velocimeter system measures only the motion of either naturally occurring or artificially generated micron size tracer particles entrained in the fluid. Its accuracy is, therefore, limited by the accuracy with which the particles follow the fluid flow. Since it is important to know how accurately the particles track the fluid, careful consideration must be given to the magnitude and direction of the particles velocity relative to the carrier fluid velocity. This report documents a theoretical investigation of the three dimensional dynamic behavior of micron size particles entrained

in gas flowing through a rotating transonic axial-flow air compressor rotor. The particle-to-gas velocity ratio and angular deviation relative to the gas are determined as functions of particle diameter, mass density, and radial position. Information of this nature is currently required for the application of LDV techniques to intrablade flow field mapping of aircraft turbomachinery.

Several previous studies (ref. 3,4,5) have investigated particle tracking for LDV applications but have been restricted to particle flow in such systems as turbulent flows, nozzles, oscillating gases, shock waves, and over airfoils. Reference 6 used a LDV system to measure the velocity lag of aerosol particles in small supersonic nozzles and then used this information in conjunction with numerical predictions to determine particle size. A theoretical study by Hussein and Tabakoff (ref. 7) and an experimental study by Tabakoff et al. (ref. 8) provide trajectories and velocities of solid particles suspended in a gas passing through an axial flow turbine stage. The objective of their investigations was to estimate the flow properties of a gas-particle suspension flowing over turbine blades. This information would ultimately be used to minimize blade erosion in dusty environments through appropriate redesign. Since their work considered particle diameters generally ranging from 100-900 microns, their results are inapplicable for LDV applications because of the resulting high velocity lags. Wisler and Mossey (ref. 2) obtained detailed flow field measurements within the rotating blade row of a low speed axial

compressor using a laser-Doppler velocimeter. Their measurements generally agreed to within 2-3 percent with hot film and pitot-static probe measurements outside the blade row, and with potential flow solutions near the leading edge. Their work was restricted to flow velocities sufficiently low that particle velocity lag was not regarded as a significant problem. However, as gas flow velocities and accelerations increase, particle velocity lag in blade channels becomes more significant, and application of LDV techniques to flow field mapping should be guided by the results of a dynamic analysis of similar gas-particle flow systems.

A two-dimensional dynamic analysis of micron size particles entrained in high Mach number subsonic gas flow passing through a stationary cascade of turbine stator blades was conducted by the author in reference 9. The particle-to-gas velocity ratio and particle angular deviation relative to the gas were determined as functions of particle size and mass density. Results indicated that velocity and angular deviations generally less than 1 percent and 0.5 degree respectively, could be achieved with 1 gm/cc tracer particles with diameters of 0.5 microns or less. The results were restricted, however, to a nonrotating blade configuration with a constant meridional streamline radius, and were not necessarily applicable to rotating systems with variable streamline radius.

GAS-PARTICLE FLOW SYSTEM

The flow system analyzed in this investigation is the three-dimensional gas-particle flow through a transonic axial-flow air compressor rotor. The rotor is currently being tested at the

NASA-Lewis Research center as part of a program to reduce the size and weight of fans and compressors while maintaining high levels of performance. The rotor was designed for a weight flow per unit annulus area of 198 kg/sec-m^2 (40.6 lbm/sec-ft^2), a tip speed of 424 m/sec (1393 ft/sec), a total pressure and temperature ratio of 1.601 and 1.162 respectively, and a tip solidity of 1.30. This resulted in a rotor with 44 blades each with a 2.5 aspect ratio, a leading edge tip diameter of .5038m (1.653 ft.), a hub-to-tip radius ratio of 0.504, and a rotational speed of 16,100 revolutions per minute. A photograph of the rotor is shown in figure 1. Performance data and blade-element design parameters are presented in reference 10.

Analysis of the gas-particle flow through the transonic compressor rotor in figure 1 is conducted from a radius of 60 to 94 percent of the blade span as measured from the rotor axis. Analysis was not made below 60 percent span because each blade has a vibration damper located at about 55 percent span which precludes the use of LDV techniques below that level.

TECHNICAL APPROACH AND ANALYSIS

Analysis of the gas-particle flow field was conducted in two separate steps. In the first, the magnitude and direction of the gas velocity was determined at all points of a blade channel in the 60-94 percent span range. In the second, the magnitude and direction of the particle velocity was determined throughout the region by analyzing the path followed by particles in a three-dimensional flow field with a known gas velocity distribution.

Decoupling the gas and particle flows in this way is justified because of the low mass fraction of naturally occurring or artificially generated aerosols in most LDV gas-dynamic applications. Therefore, since the particles do not influence the gas flow, the particles and gas may be analyzed separately.

GAS FLOW ANALYSIS

The three-dimensional gas flow field was determined with a numerical technique developed by Kurzrock and Novick (ref. 11) which yields a solution for steady, transonic blade element flow in an axial compressor rotor. The equations governing the flow in a rotating blade row are formulated as an abbreviated form of the Navier-Stokes equations with the dominant viscous terms retained to allow for the formation of embedded shock waves in the flow field. The coordinate system used is an orthogonal curvilinear system attached to the rotor. The independent variables are the meridional streamline distance m and the tangential angle θ. For purposes of analysis, finite solution regions are chosen on blade-to-blade surfaces. These regions are bounded on the top and bottom by adjacent blade surfaces and by arbitrarily chosen upstream and downstream boundaries. Figure 2 illustrates a blade-to-blade surface of revolution, a typical solution region, and the coordinate systems used in this study. A stream channel is defined by specifying a meridional streamline radius and the stream channel thickness as functions of the meridional distance. It is assumed that the radius varies linearly with the axial distance. Therefore, the angle between any stream surface and the rotor axis as measured

in the meridional plane is constant and is referred to as the cone angle λ.

Gas flow field analysis was conducted on stream surfaces at 60, 69.2, 77.8, 86.2, and 94.3 percent radial span. The governing equations are derived in reference 11 for the meridional-tangential relative frame of reference shown in figure 2. A thermally and calorically perfect gas has been assumed with constant viscosity and thermal conductivity. Shock waves are handled as a viscous phenomenon and, therefore, become "smeared" in the solution. The method of characteristics is used to determine the boundary conditions along the blade surfaces and at the exit plane. Flow tangency is enforced on the blade surfaces, and a constant back pressure is specified at the exit plane. Steady supersonic uniform flow conditions are specified along the upstream boundary, and periodicity is enforced on the remaining free surfaces of the solution region.

The entire numerical technique is incorporated into a computer code designated ROTOR. The code is written in FORTRAN IV for use on the IBM 370/165 and CDC 6600 digital computers, and was modified in this study for use on the Xerox Corporation Sigma 7 computer. The input to ROTOR requires the m-θ blade coordinates on the stream surface being analyzed, and the compressor flow conditions. The output includes the relative meridional velocity, tangential velocity, flow angle measured from the axial-radial plane, and Mach number at each grid point of a network established for finite difference analysis.

PARTICLE FLOW ANALYSIS

From Newton's second law of mechanics the vector equation of motion of a single, spherical particle moving with an absolute velocity u_g is

$$\frac{\pi D^3}{6} \rho_p \bar{a}_p = \frac{C_D}{2} \rho_g \frac{\pi D^2}{4} (\bar{u}_g - \bar{u}_p)^2 \qquad (1)$$

The term on the left denotes the mass times the absolute acceleration of the particle and represents the force required to accelerate the particle in the absence of potential force fields. The term on the right represents the total viscous drag exerted on the particle by the surrounding fluid and is expressed in terms of an empirically determined viscous drag coefficient C_D. Equation (1) assumes that the force on the particle caused by the pressure gradient in the surrounding fluid, the force required to accelerate the apparent mass of the particle relative to the fluid, and the force which accounts for the deviation of the flow from steady state (Basset force) are negligible. These assumptions are justified (ref. 5,7) in flow systems whose properites are changing very gradually or when the particle density is much larger than the fluid density. Both of these conditions are generally satisfied in this study. It is also assumed that the particles are non-interacting and uniformly distributed within the carrier gas and that there are sufficiently few particles that their presence does not alter the gas properties from that of the gas flow alone. These assumptions are valid for most LDV applications employing

naturally occurring or artifically generated aersols.

Letting $C_D = 24\psi(Re, M)/Re$, where $\psi(Re, M)$ is a Reynolds-Mach number dependent function which accounts for deviation of the drag coefficient from the ideal Stokes flow value (24/Re), equation (1) becomes:

$$\bar{a}_p = \beta\ (\bar{u}_g - \bar{u}_p) \qquad (2)$$

where $$\beta = \frac{18\mu\psi(Re,M)}{D^2\rho_p}.$$

In order to derive the differential equations of motion of a particle passing through a rotating blade row of a compressor rotor, the coordinate systems o'lr θ and oxyz are defined and are illustrated in figure 2. The frame of reference o'lr θ is fixed in an arbitrary blade passage of the rotor and moves with constant angular velocity ω of the rotor. The coordinate directions l, r, and θ are the axial, radial, and tangential directions respectively, and are used to denote the location of a particle relative to the rotating blade row. Point O' is the origin of the relative coordinate system and is located on the rotor axis at the intersection with a perpendicular plane passing through the leading edge of the solution region. The oxyz coordinate system is an inertial frame of reference attached to the rotor axis and is composed of mutually perpendicular axes x, y, and z. The x coordinate axis is in the axial direction (l direction of the relative coordinate system) while axes y and z lie in a plane parallel to the r - θ plane of the relative system.

Assume that at time t=o the planes formed by the 1-r axes and x-y axes are coincident and a particle p is at an arbitrary position 1, r, and θ as measured from o'. As illustrated in figure 2, after time t the o'1r system has rotated about the 1 axis, and the 1-r plane is an angle of ωt from the x-y plane. At any point in time the x, y, and z components of the particles equation of motion are, from equation 2:

$$a_{px} = \beta\ (u_{gx} - u_{px})$$
$$a_{py} = \beta\ (u_{gy} - u_{py})$$
$$a_{pz} = \beta\ (u_{gz} - u_{pz}) \qquad (3)$$

The relationships between the absolute and relative axial components of the particle displacement, velocity and acceleration are seen from figure 2 to be:

$$x_p = 1$$
$$u_{px} = \dot{1}$$
$$a_{px} = \ddot{1} \qquad (4)$$

Similarly for the y and z directions:

$$y_p = r \cos(\theta + \omega t)$$
$$u_{py} = -r(\dot{\theta} + \omega) \sin(\theta + \omega t) + \dot{r} \cos(\theta + \omega t)$$
$$a_{py} = \ddot{r} \cos(\theta + \omega t) - 2\dot{r}(\dot{\theta} + \omega) \sin(\theta + \omega t) - r[(\dot{\theta} + \omega)^2 \cos(\theta + \omega t) + \ddot{\theta} \sin(\theta + \omega t)] \qquad (5)$$

$$z_p = r \sin(\theta + \omega t)$$
$$u_{pz} = r(\dot{\theta} + \omega) \cos(\theta + \omega t) + \dot{r} \sin(\theta + \omega t)$$
$$a_{pz} = \ddot{r} \sin(\theta + \omega t) + 2\dot{r}(\dot{\theta} + \omega) \cos(\theta + \omega t) + r[\ddot{\theta} \cos(\theta + \omega t) - (\dot{\theta} + \omega)^2 \sin(\theta + \omega t)] \qquad (6)$$

The absolute components of the gas velocity may be expressed in terms of the gas relative velocity components. They become:

$$u_{gx} = u_{gl}$$

$$u_{gy} = - r\,\omega \sin(\vartheta + \omega t) - u_{g\vartheta} \sin(\theta + \omega t) + u_{gr} \cos(\theta + \omega t)$$

$$u_{gz} = r\,\omega \cos(\vartheta + \omega t) + u_{g\vartheta} \cos(\theta + \omega t) + u_{gr} \sin(\theta + \omega t) \quad (7)$$

Substituting equations (4) - (7) into equation (3) and rearranging to solve for the particle relative acceleration components yields:

$$\ddot{l} = \beta\,(u_{gx} - \dot{l}) \quad (8)$$

$$\ddot{r} = \beta\,(u_{gr} - \dot{r}) + r\,(\dot{\vartheta} + \omega)^2 \quad (9)$$

$$\ddot{\vartheta} = \frac{\beta}{r}\,(u_{g\theta} - r\dot{\vartheta}) - 2\frac{\dot{r}}{r}\,(\dot{\vartheta} + \omega) \quad (10)$$

Equations (8) - (10) constitute a coupled system of second order ordinary differential equations which govern the relative motion of a particle through a rotating blade row of a turbomachine. As pointed out in reference 7, the second term in the right hand side of equation (9) accounts for the centrifugal acceleration of the particle, while the second term in the right hand side of equation (10) represents the Coriolis component of acceleration. The path followed by a particle and its velocity along that path may be determined by numerically integrating equations (8) - (10) through the gas flow field.

In the absence of reliable drag data the drag coefficient is frequently assumed to be given by the classical Stokes drag law $C_D = 24/Re$, where $Re = D\rho_g |u_g - u_p|/\mu$. Although it is most convenient to use Stokes law for the drag coefficient, it becomes

increasingly unrealistic for Reynolds numbers above approximately 1.0 and in flows where rarefaction, compressibility and inertial effects are significant. The drag coefficient used in this study is given by Carlson and Hoglund (ref. 12) and corrects the Stokes law for these effects. Therefore, it is applicable throughout the continuum, slip and transition flow regimes. The expression is

$$C_D = \frac{24}{Re}\,\psi(Re, M), \qquad (11)$$

where

$$\psi(Re, M) = \frac{(1 + .15\ Re^{.687})\ (1 + \exp(-.427/M^{4.65} - 3/Re^{.88}))}{1 + (M/Re)\ (3.82 + 1.28\ \exp(-1.25\ Re/M))}$$

acoounts for deviation from Stokes flow. The Mach number is based upon the absolute relative velocity of the gas with respect to the particles.

PARAMETRIC STUDY

The dynamic behavior of several gas-particle mixtures was determined by numerically solving equations (8), (9), and (10) with the viscous drag coefficient given by equation (11). Several cases were examined by varying the diameter and mass density of the particles over ranges selected to correspond to values encountered in most present-day LDV gas dynamic applications. The particle diameter varied from 0.5-4 microns and the mass density ranged from 1-4 gm/cc. The rotor gas flow remained constant throughout the study and was characterized by a mass flow rate of 29.5 kg/sec (65 lbm/sec), inlet mass density of 0.845 kg/m^3

(0.0527 lbm/ft^3), inlet total pressure and temperature of 3.37 N/m^2 (10.13 lbf/in^2) and 288 K(518.4R), respectively, and a specific heat ratio of 1.4. The rotor speed was constant at 16100 RPM. Particles were introduced into the flow system at initial radial positions extending from 60-94.3 percent of the radial span ($.198 < r < .241$ m). The relative gas Mach numbers at the point of particle injection ranged from 1.15 at the 60 percent span point to 1.31 at the 94.3 percent span point. The particles were assumed to possess an initial velocity equal to 99 percent of the corresponding gas velocity and to have no angular deviation relative to the gas. Their velocities and trajectories were numerically determined as they progressed through the blade channel. Analysis of a particlar particle was continued until either it passed through the rotor or until it entered the near-blade region. This is defined as the region between the finite difference grid network and a blade surface. Since particles which entered this region were generally large and dense, and therefore unsuitable for LDV applications, their analysis was terminated immediately after entering the region. In an actual blade channel, particles which enter the near-blade region normally collide with the adjacent blade surface and rebound back into the flow stream with an increased velocity lag and angular deviation relative to the gas. In practice, LDV electronics systems are generally designed to descriminate against such particles either because of their large size or because their velocities are significantly different from the mean velocity of the surrounding particles.

GAS FLOW RESULTS

The three-dimensional gas flow field was determined with the numerical technique of reference 11 on blade-to-blade stream surfaces corresponding to 60.0, 69.2, 77.8, 86.2, and 94.3 percent radial span based upon the radius at the leading edge. Stream surfaces are approximated by conical surfaces of revolution with their apexes on the compressor axis of rotation. They are characterized by radii at the leading and trailing edges of the blade row respectively, and by their cone angle. Table I summarizes the stream surfaces examined in this study.

The flow fields on the 94.3, 77.8, and 60.0 percent span stream surfaces are illustrated in figures 3, 4, and 5 by relative intrablade Mach number vectors. They are located at each finite difference grid point within the solution region. The regions are presented in terms of nondimensional

TABLE I

GAS FLOW SOLUTION REGIONS

Radial Position	Radius at Leading Edge, m	Radius at Trailing Edge, m	Cone Angle, Deg.	Percent Span
RP2	.242	.238	-8.227	94.3
RP3	.232	.229	-6.120	86.2
RP4	.222	.220	-3.946	77.8
RP5	.211	.210	-1.705	69.2
RP6	.200	.202	.642	60.0

meridional and tangential coordinates respectively. The axial and radial velocity components at each grid point are determined from the meridonal component and the stream surface cone angle.

The gas velocity at any axial, radial and tangential position within the three-dimensional rotor blade channel is determined with an interpolation routine based upon flow field information on the stream surfaces of Table I. Table II summarizes average flow field information across the entrance and exit of the solution regions.

TABLE II

AVERAGE ENTRANCE AND EXIT FLOW CONDITIONS

Radial Position	Entrance Relative Mach Number	Exit Relative Mach Number	Entrance Relative Flow Angle, Deg.	Exit Relative Flow Angle, Deg.
RP2	1.318	.885	65.24	60.66
RP3	1.281	.826	63.62	57.19
RP4	1.241	.770	62.10	54.32
RP5	1.199	.714	60.60	50.85
RP6	1.153	.667	59.06	47.10

Figures 3-5 provide justification for the following conclusions regarding the three-dimensional gas flow field relative to the blade:

a) the intrablade velocity increases with radial span,

b) the inlet flow field is supersonic and the outlet flow field is generally subsonic,

c) there is generally a smooth turning of the flow through the blade channel,

d) there is a deviation in the smooth transition of flow angle near the leading edge of the pressure surface and the trailing edge of the suction surface.

e) On each stream surface the velocity decreases as the tangential position increases at constant meridional position from the suction surface to the pressure surface,

f) the relative Mach number adjacent to the leading edge of the suction surface varies with radius from 1.28 to 1.69, and the relative Mach number adjacent to the trailing edge of the pressure surface varies from 0.3465 to 0.687.

PARTICLE FLOW RESULTS

The results of numerically integrating eqns. (8) - (10) through the rotating blade channel are summarized in figures 6 - 20. Figures 6 - 8 present several particle trajectories projected onto the axial-tangential coordinate surface. The trajectories are shown relative to the blade, and the average radial coordinate of the trajectories is 0.220 m (.721 ft.). It will be subsequently shown that these trajectories lie essentially in the 77.8 percent radial span (RP4) gas stream surface. Figures 9 and 10 show several trajectories plotted on the axial-radial coordinate plane.

Figures 6 and 9 present a family of trajectories of 1 micron diameter particles with a mass density of 1 gm/cc. The trajectories shown in figure 6 are typical of those obtained throughout the study and represent the approximate range of trajectories examined which did not intersect either the upper or lower near-blade region. The trajectories in figure 9 closely parallel the intersection of the gas stream surfaces of Table I with the axial-radial plane (shown as dashed lines). Therefore the particles move essentially on gas stream surfaces.

The influence of particle diameter and mass density is shown in figures 7, 8, and 10. Figures 7 and 8 indicate that an increase in either parameter causes an extension or lagging of the trajectory on the axial-tangential surface and this results in a corresponding increase in the velocity lag and angular deviation between the particles and the gas. While the results shown in Figures 7 and 8 are for a particle mass density and diameter of 1 gm/cc and 1 micron respectively, the results are typical of all other cases examined. It's seen that the curved particle path on the $1 - \theta$ surface is more sensitive to an increase in particle size than to a corresponding increase in mass density. This is justified by noting from equation (2) that if Stokes flow prevailed ($\psi(Re, M)=1$), the particle diameter and mass density would appear to the second and first power respectively. Under these conditions a doubling of the diameter would have the same effect as a 4 to 1 increase in mass density. While Stokes flow does not always occur in this study, the above anology remains essentially valid since the drag expression given by equation (11) is based upon the Stokes drag law.

Figure 10 illustrates the superposition on the axial-radial plane of several particle trajectories resulting from particles of differing diameters and mass densities. As in the case of figure 9, these particle paths lie essentially on gas stream surfaces. The results clearly indicate that within the range of particle diameters and densities examined, the radial variation of a particle passing through a rotating blade channel is

independent of the size and density of the particle. An examination of the magnitude of the centrifugal acceleration term in equation (9) shows it to be small relative to the other term, thereby confirming this result.

The tangential variation of particle-to-gas velocity ratio and particle angular deviation at three axial positions is illustrated in figures 11-14 as a function of particle diameter and average radial position. The abscissa is the normalized tangential position and is 0 at the suction surface and 1 at the pressure surface. The velocity ratio is defined as the magnitude ratio of the particle velocity to gas velocity V/U where V and U are the absolute particle and gas velocities respectively. Radial velocity components are not included in the determination of V and U since an LDV system normally views the blade channel from the radial direction, and is therefore not able to measure the radial component. Particle angular deviation ϕ is defined as $\phi = |\alpha_p - \alpha_g|$ where the flow angles α_p and α_g are based on the absolute axial and tangential velocity components. These parameters characterize the dynamic behavior of a particle at a particular point in the fluid flow. Particle velocity lag is defined as $|U - V|/U$ and is a related alternate parameter. Such a parameter does not however indicate whether the particles are moving faster or slower than the surrounding gas. LDV applications typically require that $.99 \leq V/U \leq 1.01$ and $\phi \leq .5$ degree. The tangential profiles of V/U and ϕ do not extend the full tangential width of the stream channel because of the intersection of the outer trajectories with the near-blade region and the channeling

(contraction) effect of trajectories with increasing axial streamlength and particle size.

Figures 11-14 provide justification for the following conclusions regarding particle velocity lag and angular deviation:

a) particle velocity lag decreases ($V/U \rightarrow 1$) when the particle diameter decreases, when the radial position increases, or when the middle of the blade channel is tangentially approached from either blade surface.

b) particle velocity lag and angular deviation are generally worst near the pressure surface at the entrance to the blade channel. Angular deviation is also large near the suction surface for axial positions greater than approximately $l/L = 0$,

c) particle angular deviation becomes increasingly smaller as the particle size decreases and as the middle of the blade channel is tangentially approached from either blade surface,

d) minimum angular deviation and velocity lag occur generally in the central portion of the blade channel where $l/L = 0$ and $0.4 \leq \bar{\theta} \leq 0.6$.

An additional result observed, although not illustrated in figures 11-14, was that doubling the particle size causes approximately the same change in V/U and ϕ as a 4 to 1 increase in mass density. Therefore, the particle path would remain essentially unchanged if the particle diameter was halved while at the same time increasing its mass density by a factor of 4. This result was also noted and graphically demonstrated in reference 9.

Figures 15-20 illustrate the tracking capability of particles in blade channels at three different average radial spans. The particle diameters varied from 0.5-2 microns and the mass density remained constant at 1 gm/cc. Tracking is graphically shown by lines of constant velocity ratio V/U and angular deviation ϕ. The steepest gradients in V/U occur near the leading edge of the blade channel and in the region immediately before the leading edge. The high gradients in these regions are attributed to the sudden stream channel contraction and a "smeared" bow shock in front of the leading edge of the suction blade surface.

The areas of greatest velocity lag occur generally in several well defined regions or pockets. One region is adjacent to the leading edge and another is just prior to the trailing edge of the suction surface. These are high blade-curvature regions and the particles are moving slower than the gas ($V/U < 1$) and are attempting to catch up. Two other high-lag areas are located immediately in front of the pressure surface leading edge and in a narrow oblique area in front of the blade channel. Particles in these respective areas are actually moving faster than the gas ($V/U > 1$) because of the sudden gas deceleration near the leading edge of the pressure surface, and deceleration across the "smeared" bow shock.

Minimum velocity lag generally occurs near the entrance to the flow region where the gas-particle mixture was introduced and in the region beyond the blade channel. A broad area of good particle tracking is also seen to lie in the upper central portion

of the blade channel near the pressure surface. Figures 15-17 indicate that velocity particle lags of 0.5 and 1 micron diameter particles are generally one percent or less in most regions of the blade channel. Two micron diameter particles are generally characterized by velocity lags of two percent or greater. These results remain essentially valid regardless of the radial position.

Figures 18-20 indicate that the regions of greatest angular deviation occur near the leading edge of both blade surfaces and near the trailing edge of the suction surface. Minimum angular deviation occurs near the entrance to the flow region and in the central portion of the blade channel. A generalized conclusion regarding particle-gas angular deviation for most locations within the blade channel is that the angular deviation is 0.5 and 1 degree or less, respectively, for 0.5 and 1 micron diameter particles, and greater than 1 degree for 2 micron particles.

CONCLUSIONS

The results of this investigation have provided information regarding the dynamic behavior of micron size particles moving in the three-dimensional flow field of a rotating transonic axial-flow air compressor rotor. The results indicate that particle velocity lag and angular deviation are increased whenever particle size or mass density is increased and that these parameters are more sensitive to a change in particle size than to a corresponding change in mass density. A 2 to 1 increase in particle size was found to have essentially the same effect on particle tracking as a 4 to 1 increase in particle mass density.

Plotting of particle trajectories on the axial-radial plane show that the particles move essentially on gas stream surfaces and that their radial position within the blade channel is independent of particle size and mass density. Velocity lag and angular deviation are greatest in several regions near the leading and trailing edges of the blade channel. Favorable lag and deviation occur near the entrance and exit of the solution region and in the central portion of the blade channel near the pressure surface. While particle and gas velocities are functions of radial position, particle tracking is not sensitive to the radial coordinate.

Results indicate that LDV applications employing 1 gm/cc tracer particles with diameters greater than 1 micron would experience velocity and angular deviations generally greater than 1 percent and 1 degree respectively. While these conclusions are based upon a specific transonic flow through a rotating compressor rotor with a given blade channel geometry and a fixed speed, it is felt they are also approximately valid for other high speed flows through similar compressor rotor configurations. These generalized conclusions should not be applied to regions immediately behind strong shock waves. Since shocks were assumed to be "smeared" in this study, there were no discontinuities in the gas velocity across the shocks and therefore, no high-lag relaxation zones behind them. Reference 5 showed that a relaxation zone of finite length exists behind a shock wave within which momentum exchange causes a gradual reestablishment of kinematic equilibrium between the phases. The presence of such a relaxation

zone would cause the conclusions in this study to be invalid in this region.

It should be emphasized that this study did not investigate particle flow in the boundary layers of the blade channel nor did it examine particle collision phenomena with the blade surfaces. Therefore, it is conceivable that there may be particles within the blade channel which have previously collided with a blade surface and possess a velocity and flow angle significantly different from the surrounding undeflected particles. However, reference 9 showed that unless the particles are very large and dense, the dynamic behavior of blade impacted particles is essentially indistinguishable from the behavior of the surrounding undeviated particles.

APPENDIX-SYMBOLS

a	acceleration, m/sec^2
C_D	drag coefficient
D	particle diameter, microns
L	blade chord, meters
m	meridional coordinate, meters
M	Mach number
P	pressure, N/m^2
Re	Reynolds number, $\rho_g D\|u_g - u_p\|/\mu$
t	time, sec
u	velocity, m/sec
U	absolute gas velocity, composed of axial and tangential components only, m/sec
V	absolute particle velocity composed of axial and tangential components only, m/sec
x, y, z	fixed coordinate axes
l, r, θ	axial, radial, and tangential coordinate axes of blade-fixed coordinate system or components of the relative particle position vector
$\dot{l}, \dot{r}, \dot{\theta}$	particle velocity components relative to the blade
$\ddot{l}, \ddot{r}, \ddot{\theta}$	particle acceleration components relative to the blade
α	angle formed by absolute axial and tangential velocity components, deg.
β	flow parameter, $18\ \mu\ \psi\ (Re, M)/D^2\ \rho_p$, Sec^{-1}
γ	ratio of specific heats
θ	tangential coordinate, rad
μ	gas viscosity, $N\text{-}sec/m^2$

ρ	density, kg/m^3
λ	angle between meridional streamline and axis of rotation, deg.
ϕ	absolute angular deviation between the particles and gas, $\lvert \alpha_p - \alpha_g \rvert$, deg.
$\psi(Re, M)$	Reynolds-Mach number dependent function
ω	rotor angular velocity, rev/min

Subscripts

g	gas
p	particle
x, y, z	absolute components
l, r, θ	axial, radial and tangential relative components

REFERENCES

[1]Alwang, W., Cavanaugh, L., Burr, R., and Hauer, A., "Optical Techniques for Flow Visualization and Flow Field Measurements in Aircraft Turbomachinery," PWA-3942, June 1970, Pratt and Whitney Aircraft, Hartford, Conn.

[2]Wisler, D. C. and Mossey, P. W., "Gas Velocity Measurements within a Compressor Rotor Passage Using the Laser Doppler Velocimeter," ASME Paper 72-WA/GT-2, New York, 1972.

[3]Yanta, W. J., Gates, David F., and Brown, F. W., "The Use of a Laser Doppler Velocimeter in Supersonic Flow," NOLTR 71-169, Aug. 1971, Naval Ordnance Laboratory, Silver Spring, Maryland.

[4]Karchmer, A. M., "Particle Trackability Considerations for Laser Doppler Velocimetry," TM X-2628, Sept. 1972, NASA.

[5]Maxwell, B. R. and Seasholtz, R. G., "Velocity Lag of Solid Particles in Oscillating Gases and in Gases Passing Through Normal Shock Waves," TN-D-7490, March 1974, NASA.

[6]Yanta, W. J., "Measurements of Aerosol Size Distributions with a Laser Doppler Velocimeter (LDV)," AIAA Paper No. 73-705, 1973.

[7]Hussein, M. and Tabakoff, W., "Three Dimensional Dynamic Characteristics of Solid Particles Suspended by Polluted Air Flow in a Turbine Stage," AIAA Paper No. 73-140, Washington, D. C. 1973.

[8]Tabakoff, W., Hamed, A. and Hussein, M. F., "Experimental Investigation of Gas-Particle Flow Trajectories and Velocities in an Axial Flow Turbine Stage," ASME Paper No. 72-GT-57, New York, 1972.

[9]Maxwell, B. R., "Particle Flow in Blade Passages of Turbomachinery with Application to Laser-Doppler Velocimetry," CR-134543, February 1974, NASA.

[10]Kovich, G., Moore, R. D. and Urasek, D. C., "Performance of Transonic Fan Stage with Weight Flow Per Unit Annulus Area of 198 Kilograms Per Second Per Square Meter (40.6(lbm/sec)/ft^2)," TM X-2904, Nov. 1973, NASA.

[11]Kurzrock, J. W. and Novick, A. S., "Transonic Flow Around Compressor Rotor Blade Elements, Volume I: Analysis, Volume II Digital Program User's Manual," AFAPL-TR-73-69, August 1973, Wright-Patterson Air Force Base, Ohio.

[12]Carlson, D. J. and Hoglund, R. F., "Particle Drag and Heat Transfer in Rocket Nozzles," AIAA J., Vol. 2, No. 11, November 1964, pp. 1980-94.

NASA
C-71-4254

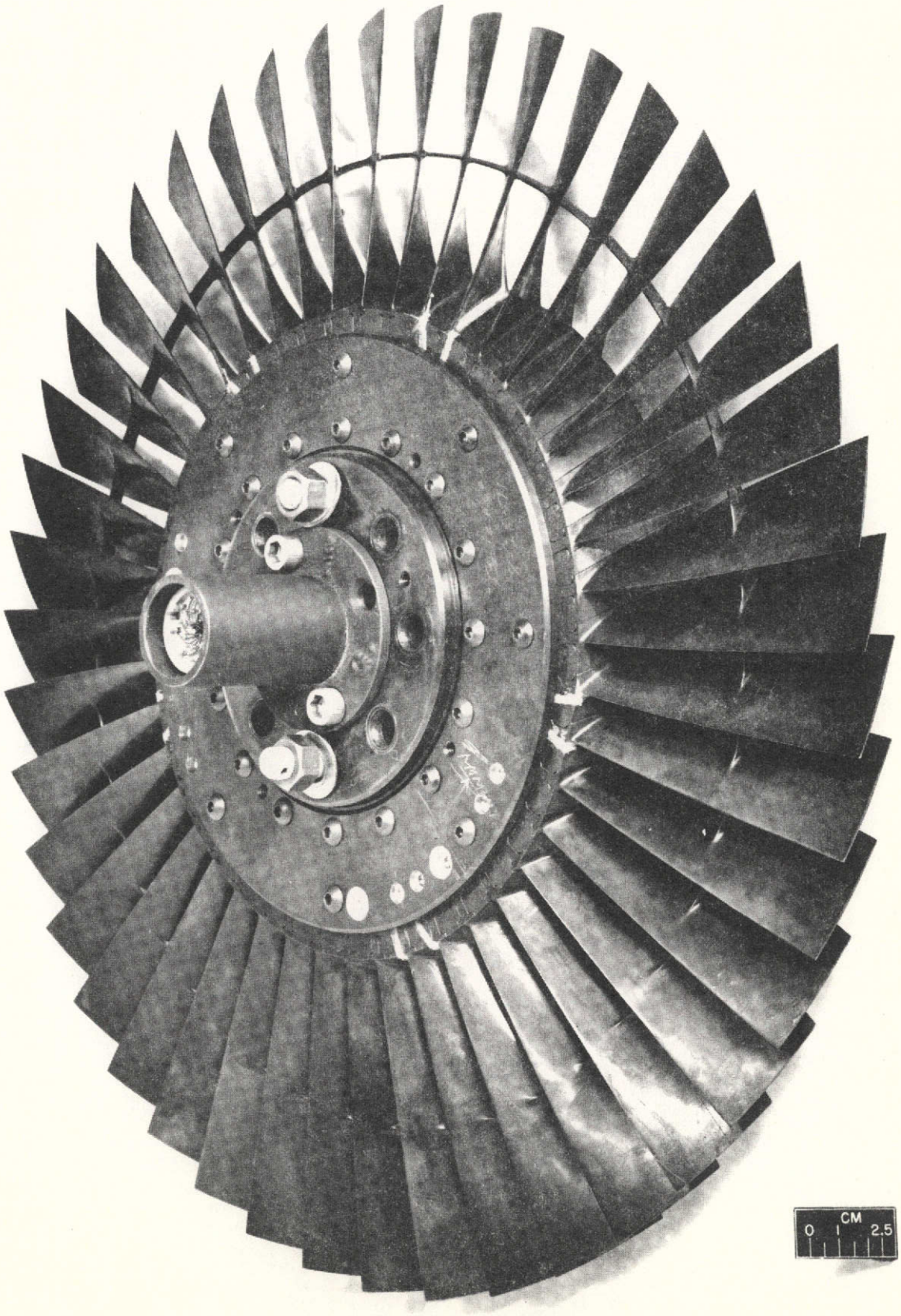

FIGURE 1 COMPRESSOR ROTOR

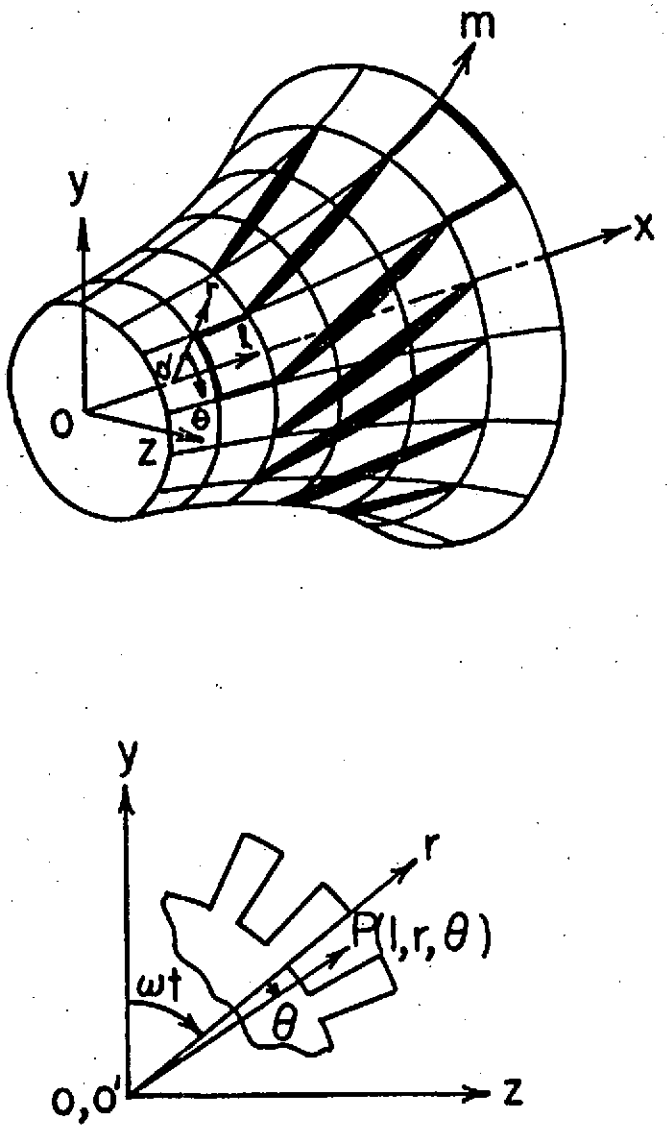

FIGURE 2 BLADE-TO-BLADE SURFACE OF REVOLUTION

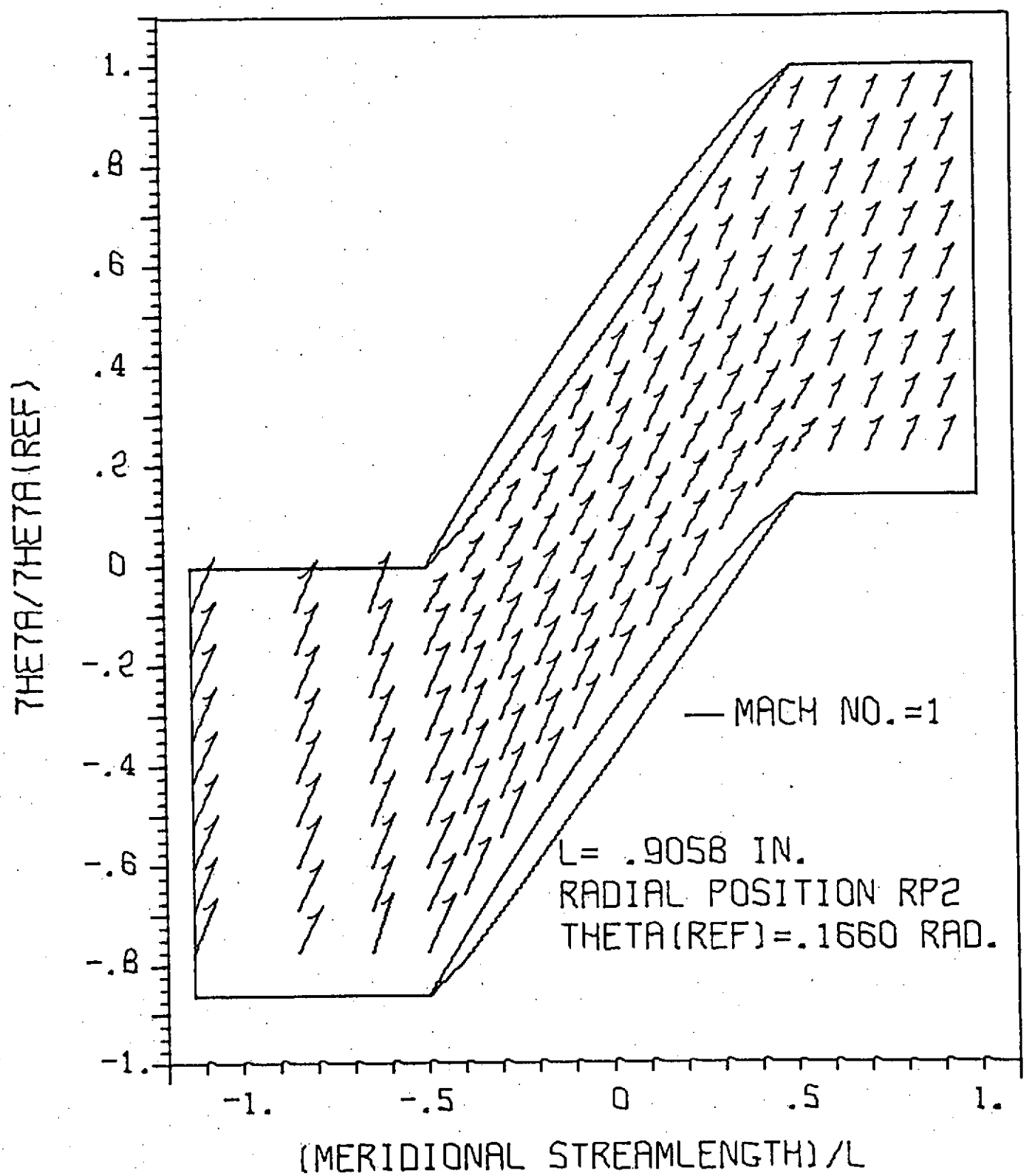

FIGURE 3 Gas Flow Field at 94.3 Percent Span

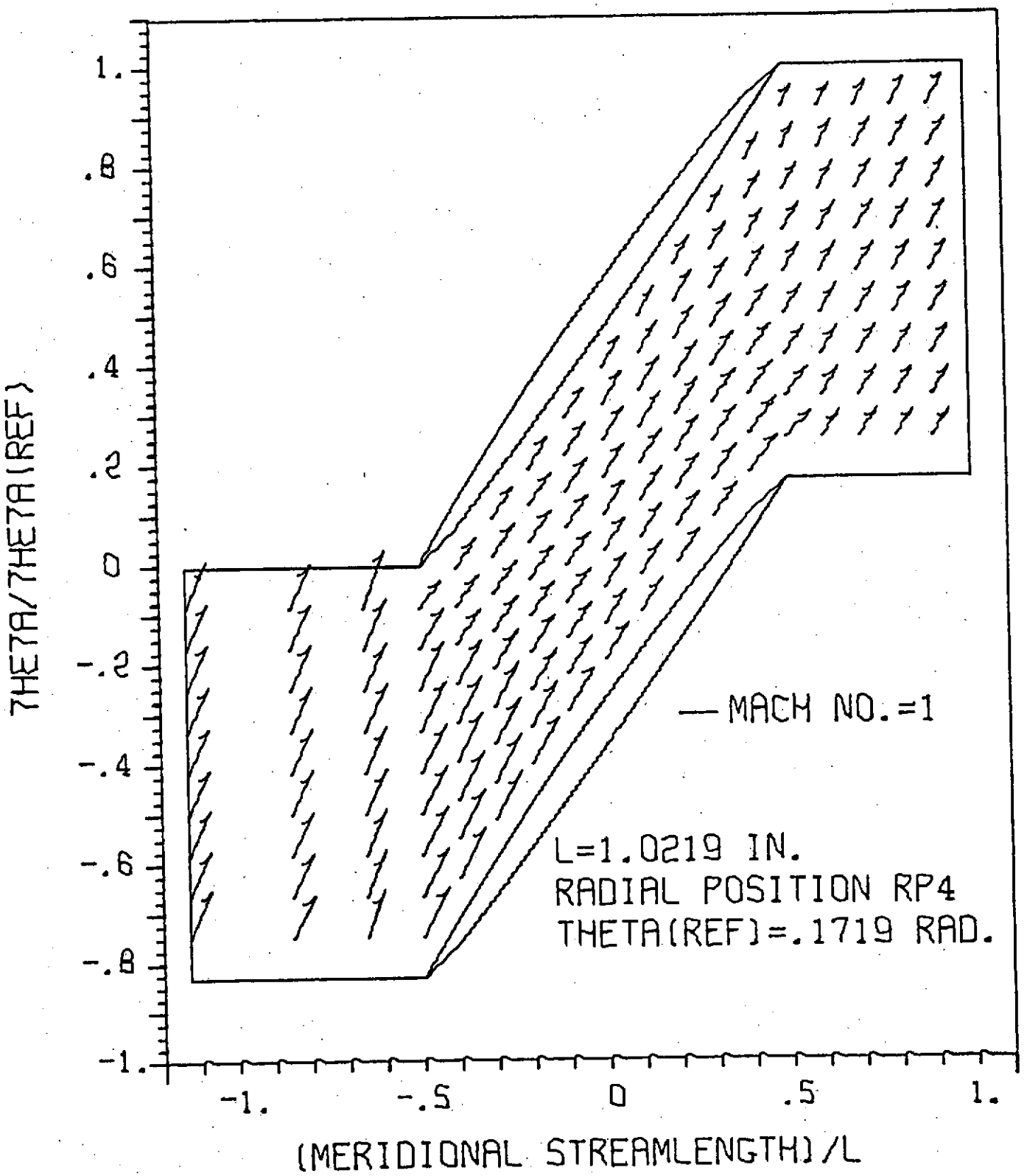

FIGURE 4 Gas Flow Field at 77.8 Percent Span

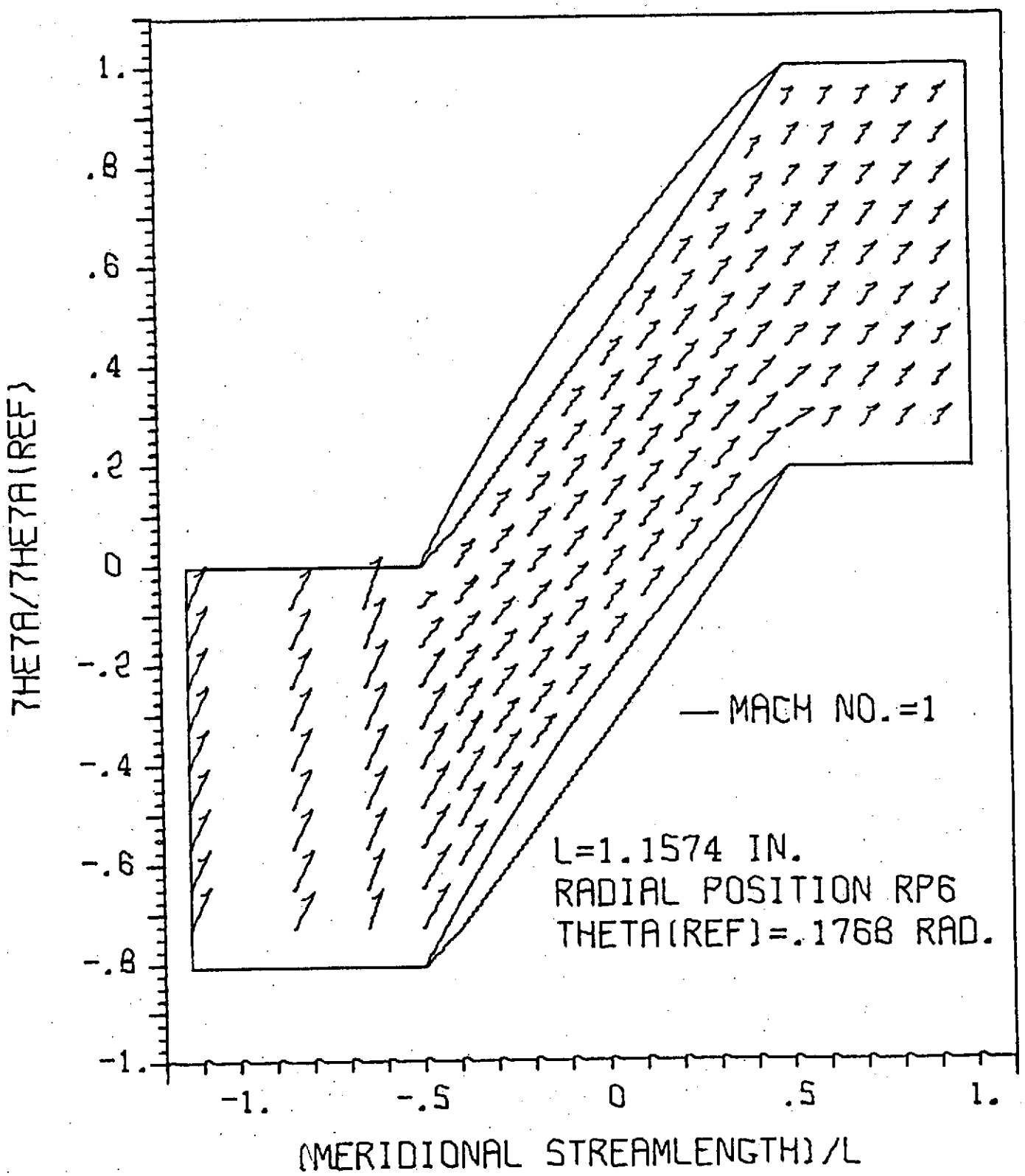

FIGURE 5 Gas Flow Field at 60.0 Percent Span

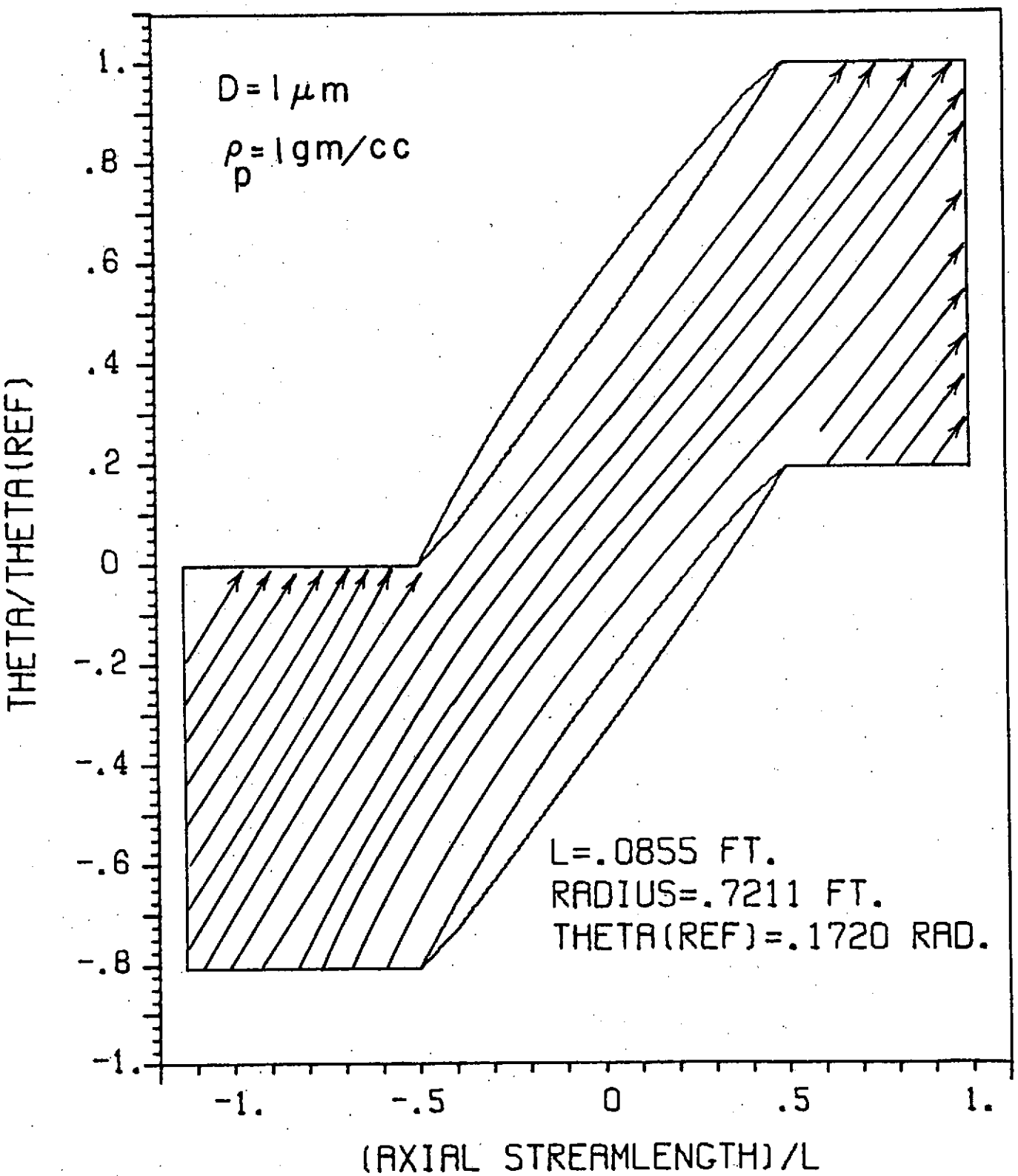

FIGURE 6 TYPICAL PARTICLE TRAJECTORIES

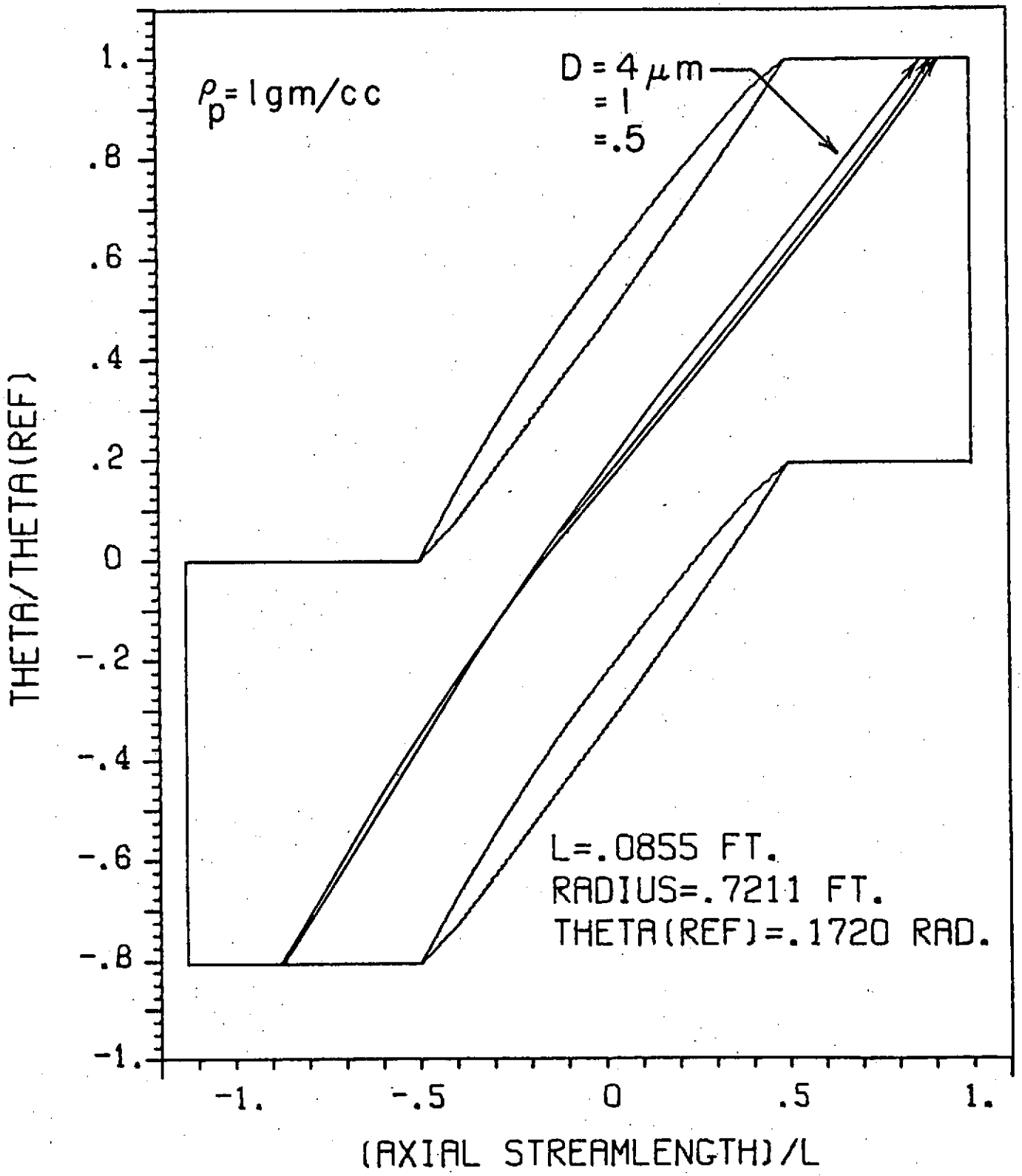

FIGURE 7 PARTICLE TRAJECTORIES AS A FUNCTION OF PARTICLE DIAMETER

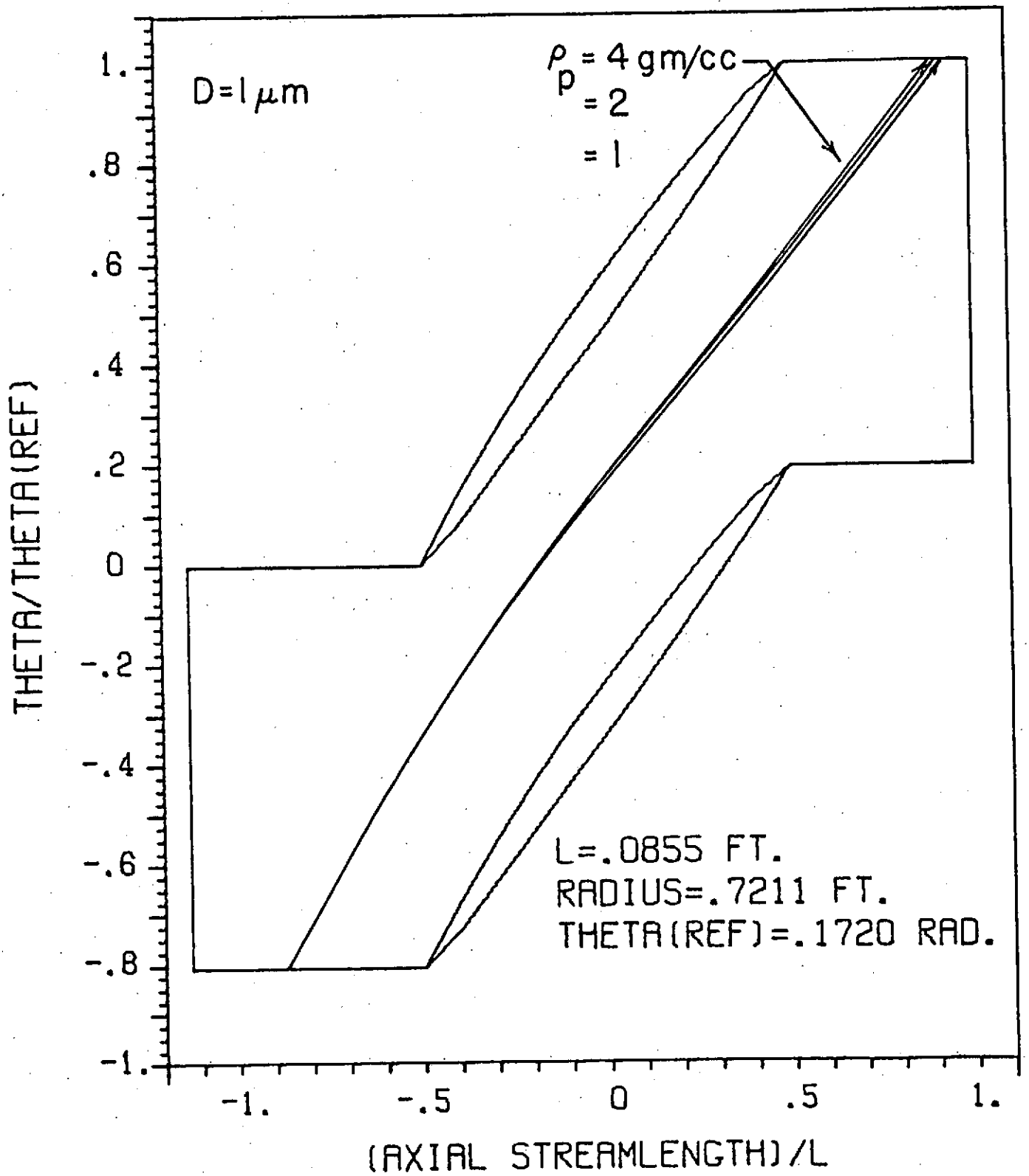

FIGURE 8 PARTICLE TRAJECTORIES AS A FUNCTION OF PARTICLE MASS DENSITY

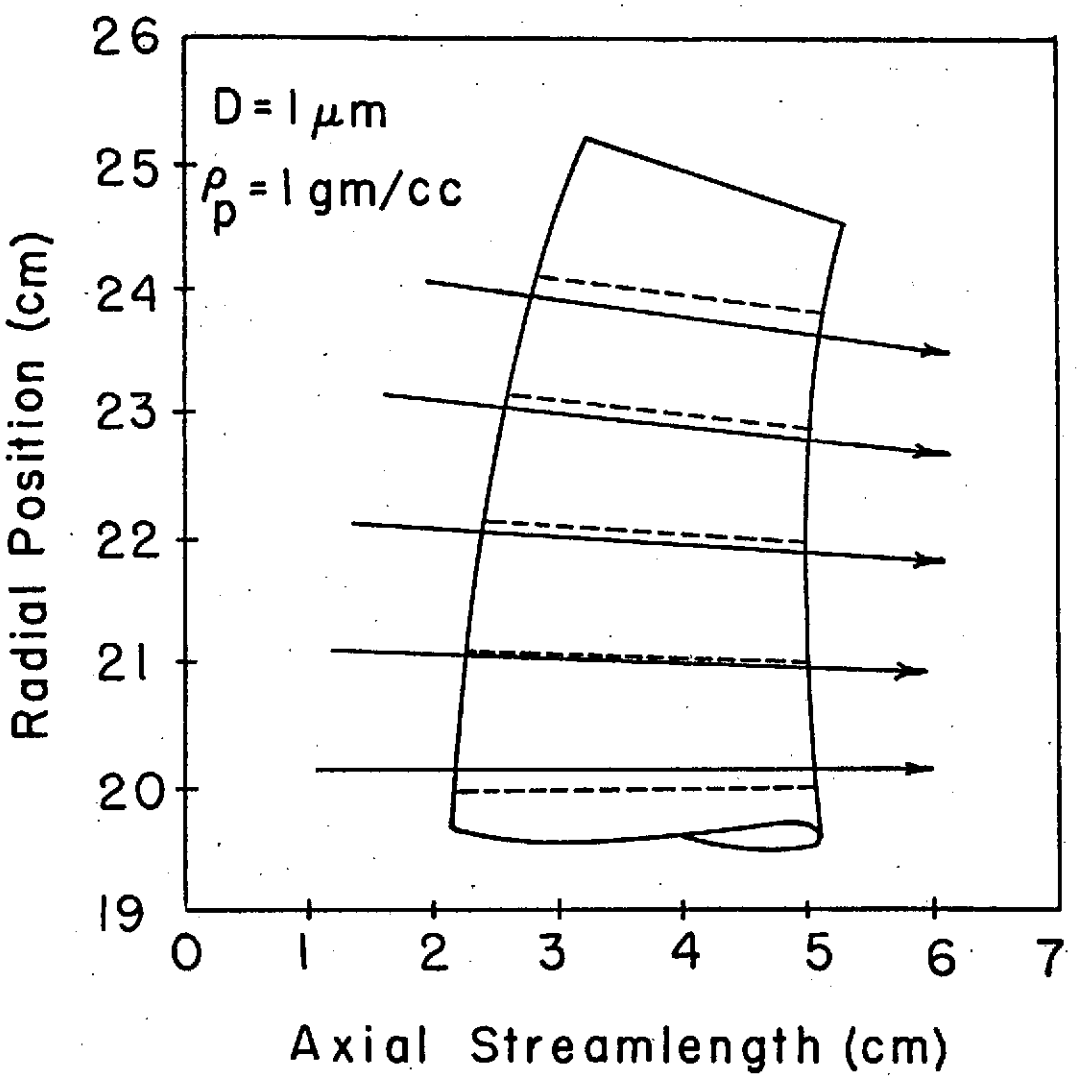

FIGURE 9 PARTICLE TRAJECTORIES ON THE AXIAL-RADIAL PLANE

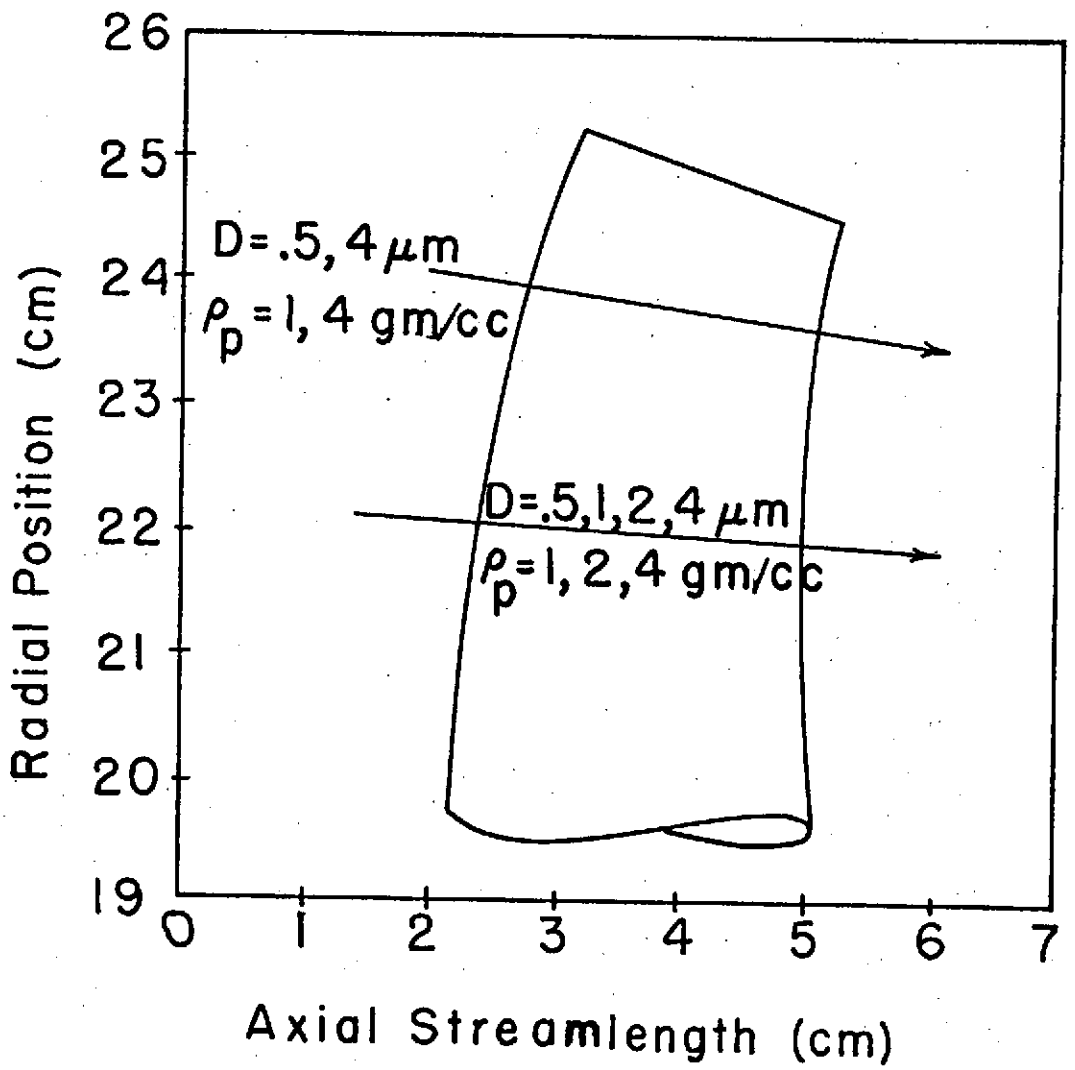

FIGURE 10 PARTICLE TRAJECTORIES ON THE AXIAL-RADIAL PLANE AS A FUNCTION OF PARTICLE PROPERTIES

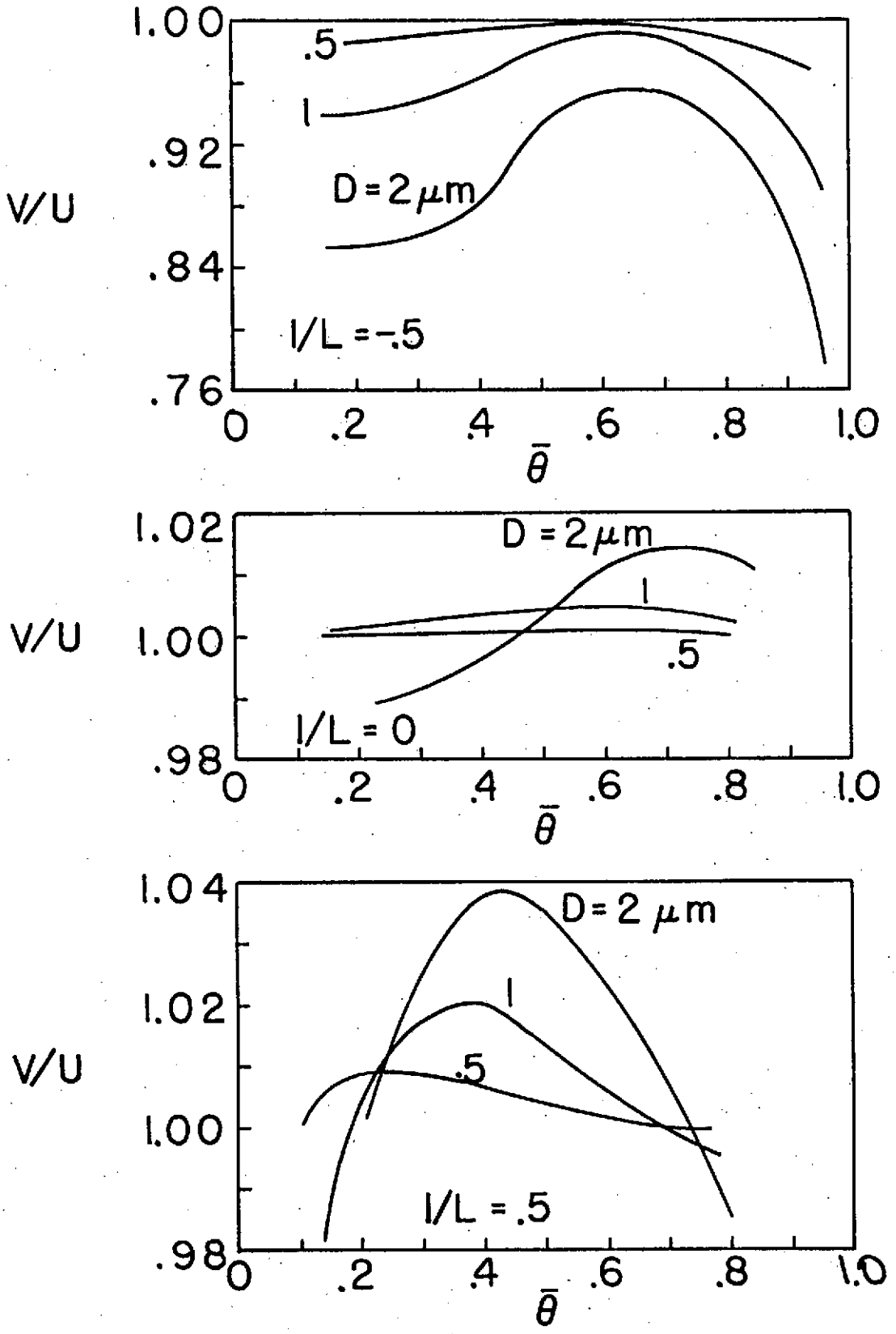

FIGURE 11 TANGENTIAL VARIATION OF PARTICLE-TO-GAS VELOCITY RATIO AS A FUNCTION OF PARTICLE DIAMETER, r = .220 m

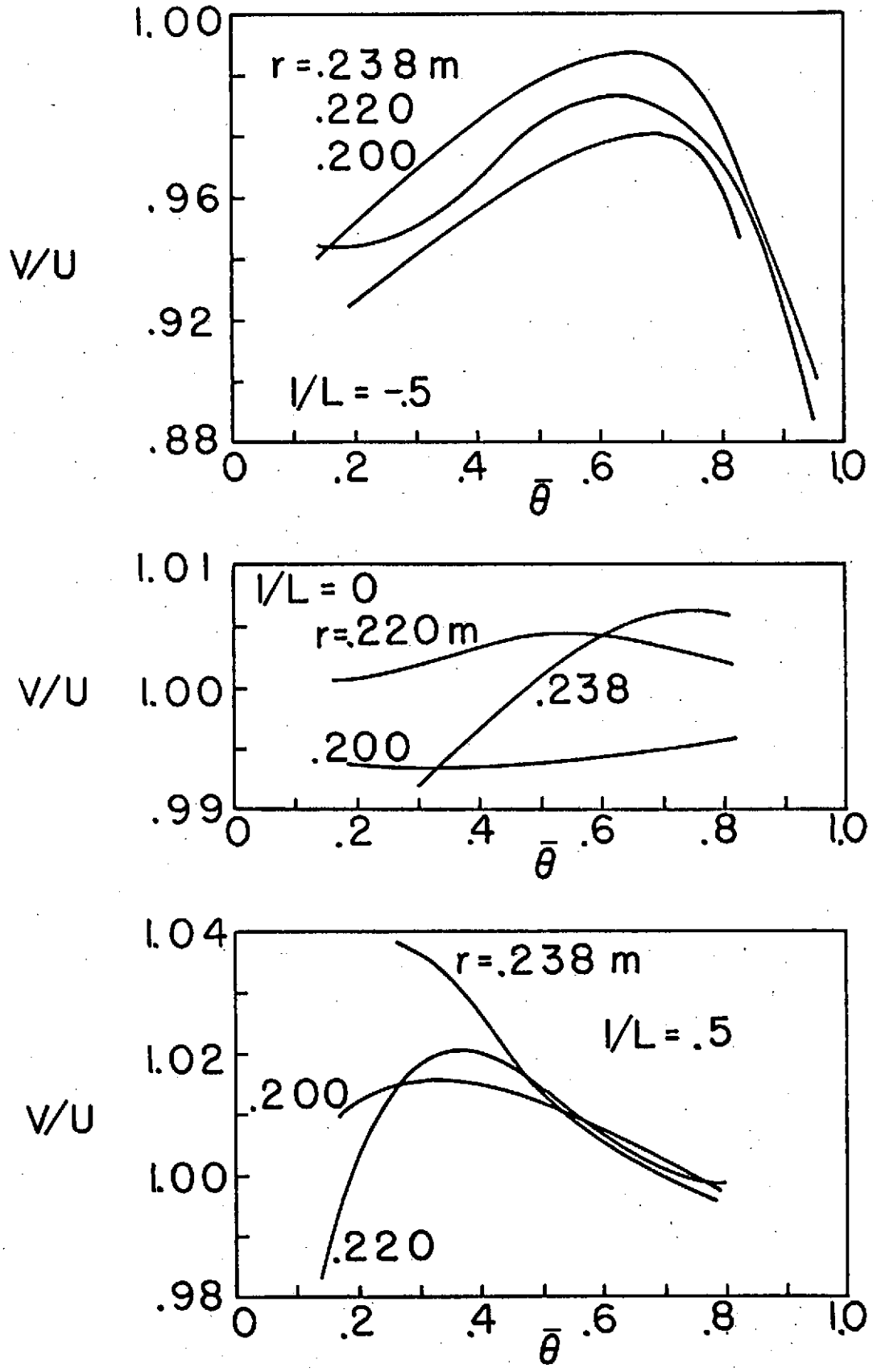

FIGURE 12 TANGENTIAL VARIATION OF PARTICLE-TO-GAS VELOCITY RATIO AS A FUNCTION OF RADIAL POSITION, D = 1 MICRON

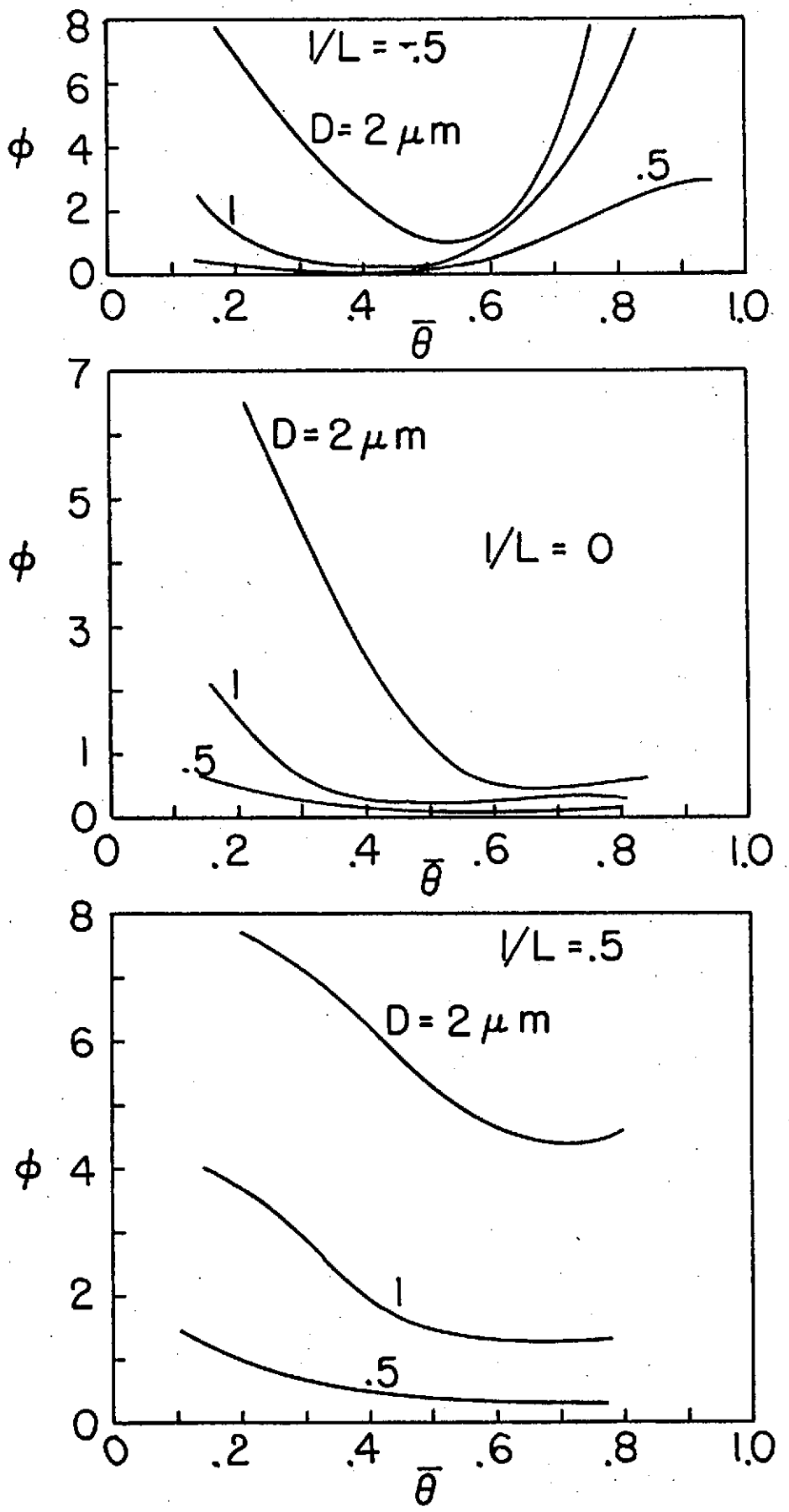

FIGURE 13 TANGENTIAL VARIATION OF ANGULAR DEVIATION AS A FUNCTION OF PARTICLE DIAMETER, r = .220 m

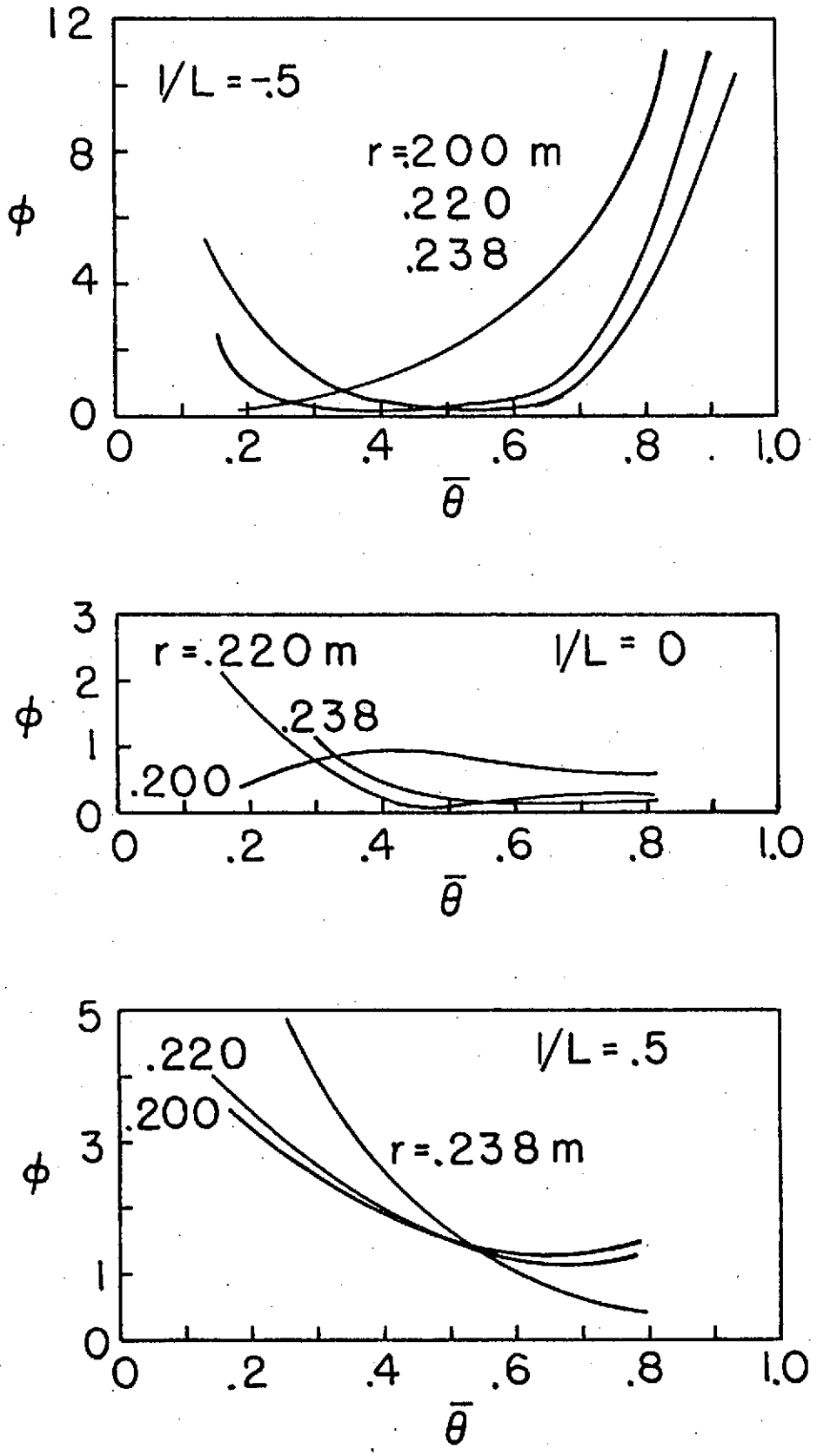

FIGURE 14 TANGENTIAL VARIATION OF ANGULAR DEVIATION AS A FUNCTION OF RADIAL POSITION, D = 1 MICRON

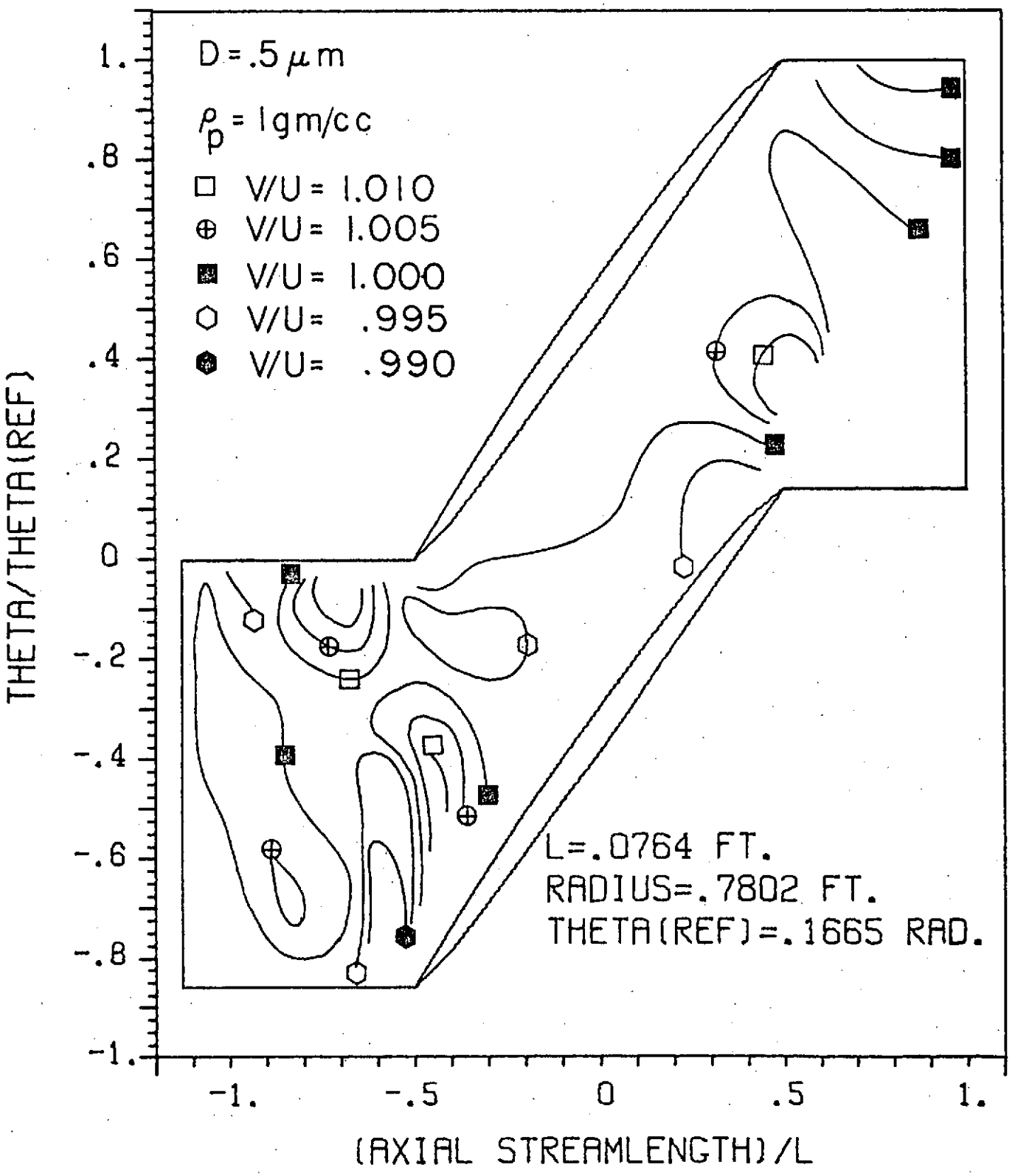

FIGURE 15A CONTOURS OF CONSTANT PARTICLE-TO-GAS VELOCITY RATIO, ρ_p = 1 gm/cc, r = .238 m

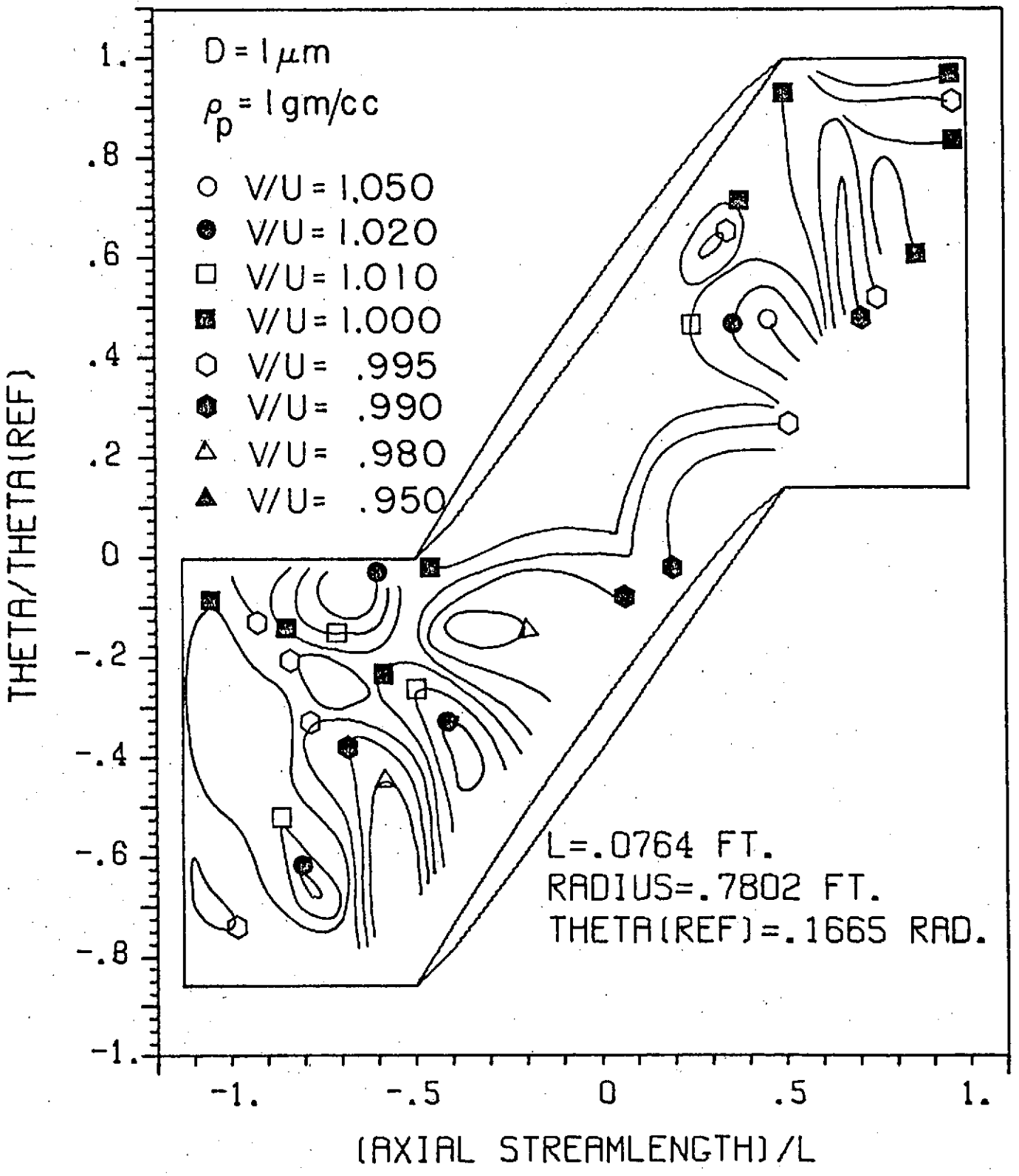

FIGURE 15B CONTOURS OF CONSTANT PARTICLE-TO-GAS VELOCITY RATIO, ρ_p = 1 gm/cc, r = .238 m

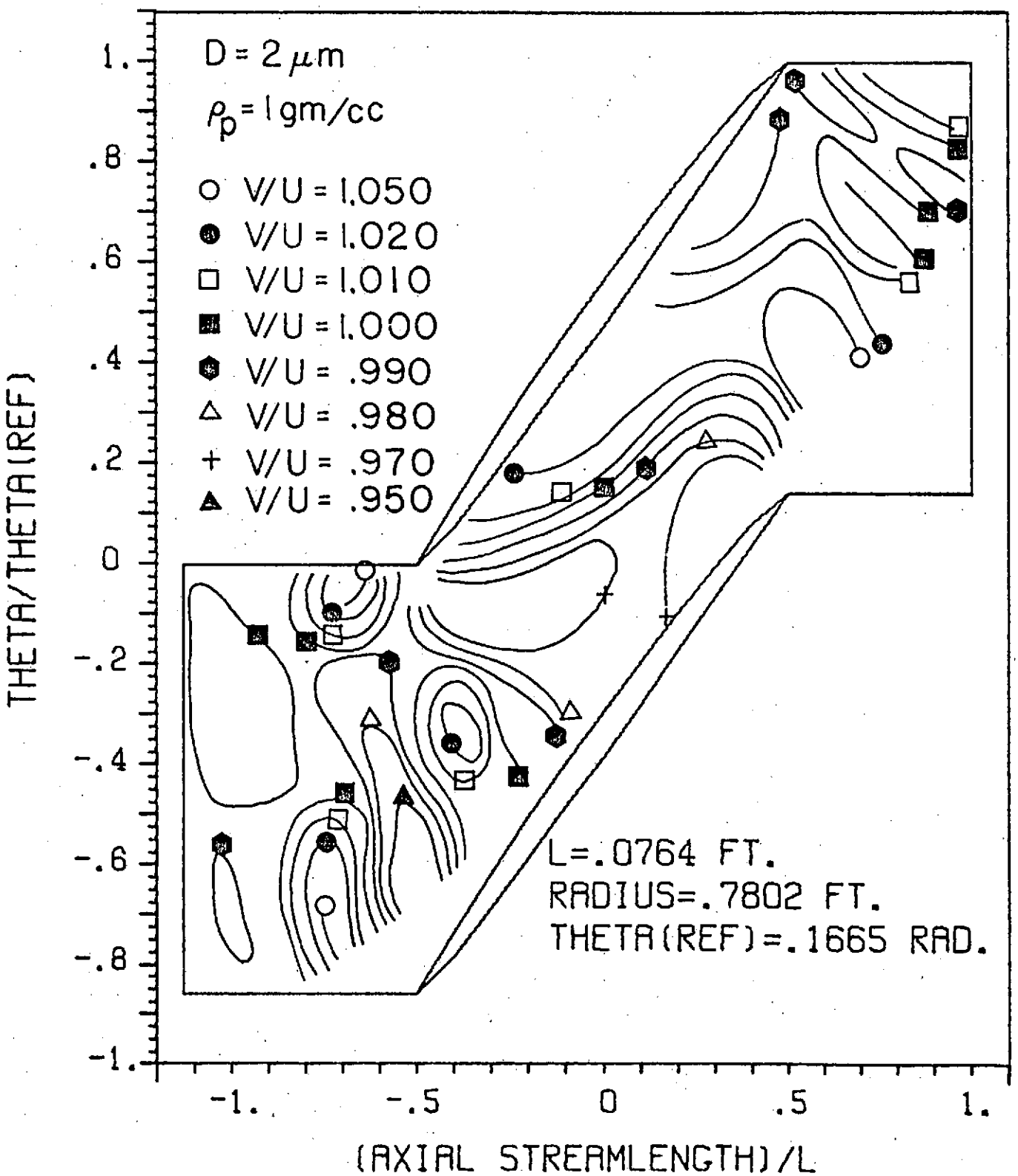

FIGURE 15c CONTOURS OF CONSTANT PARTICLE-TO-GAS VELOCITY RATIO, ρ_p = 1 gm/cc, r = .238 m

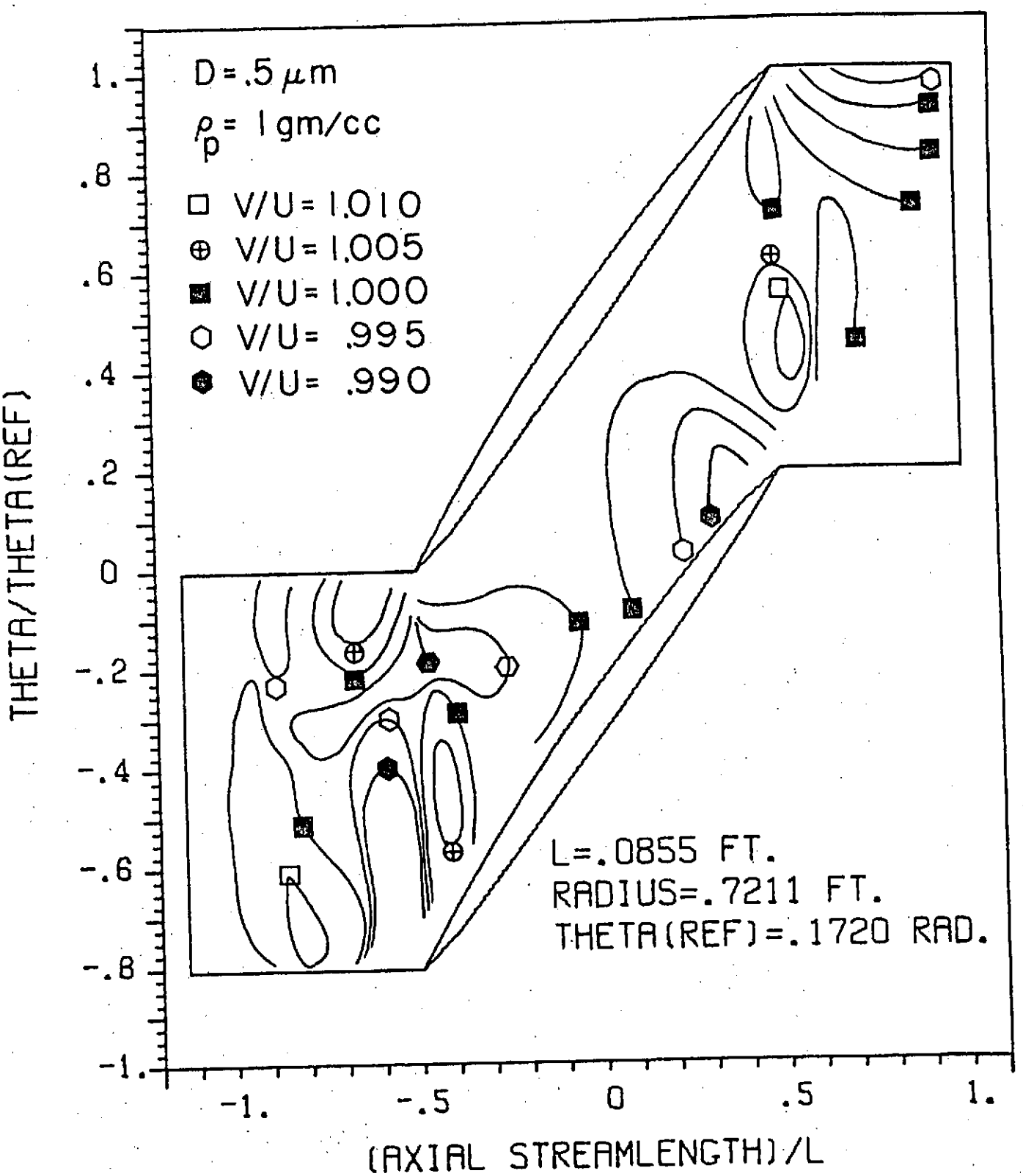

FIGURE 16A CONTOURS OF CONSTANT PARTICLE-TO-GAS VELOCITY RATIO, ρ_p = 1 gm/cc, r = .220 m

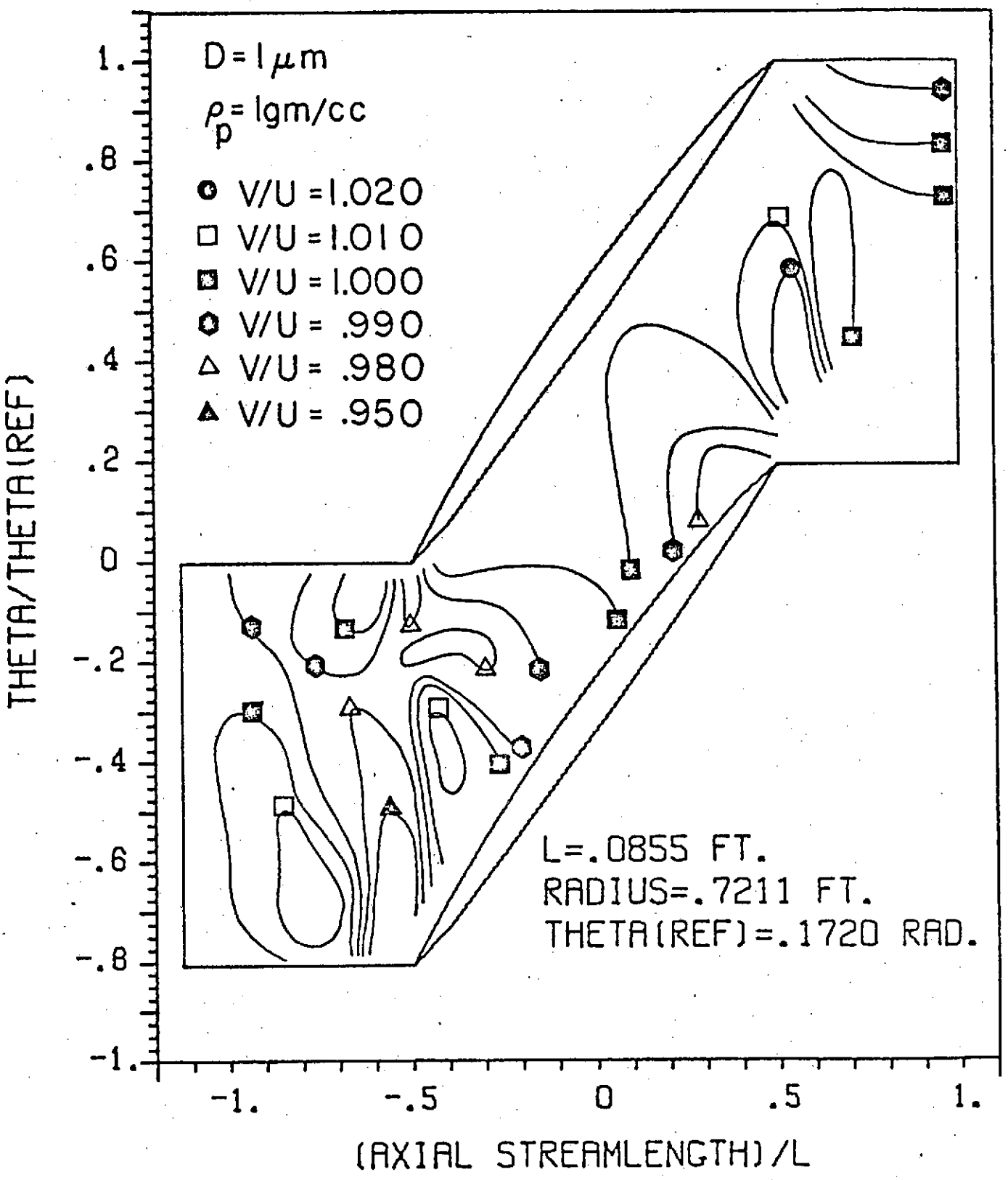

FIGURE 16B CONTOURS OF CONSTANT PARTICLE-TO-GAS VELOCITY RATIO, ρ_p = 1 gm/cc, r = .220 m

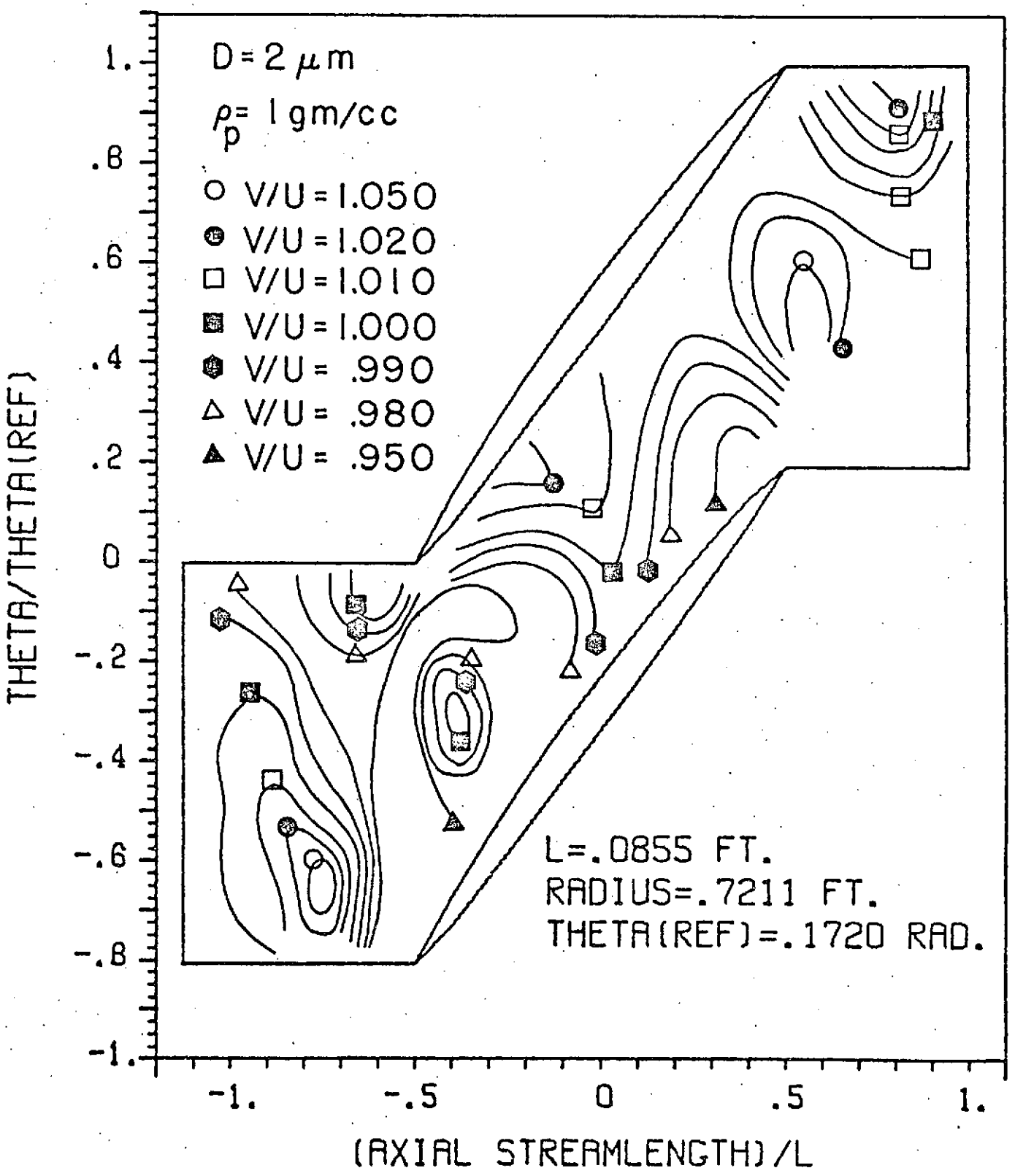

FIGURE 16c CONTOURS OF CONSTANT PARTICLE-TO-GAS VELOCITY RATIO, ρ_p = 1 gm/cc, r = .220 m

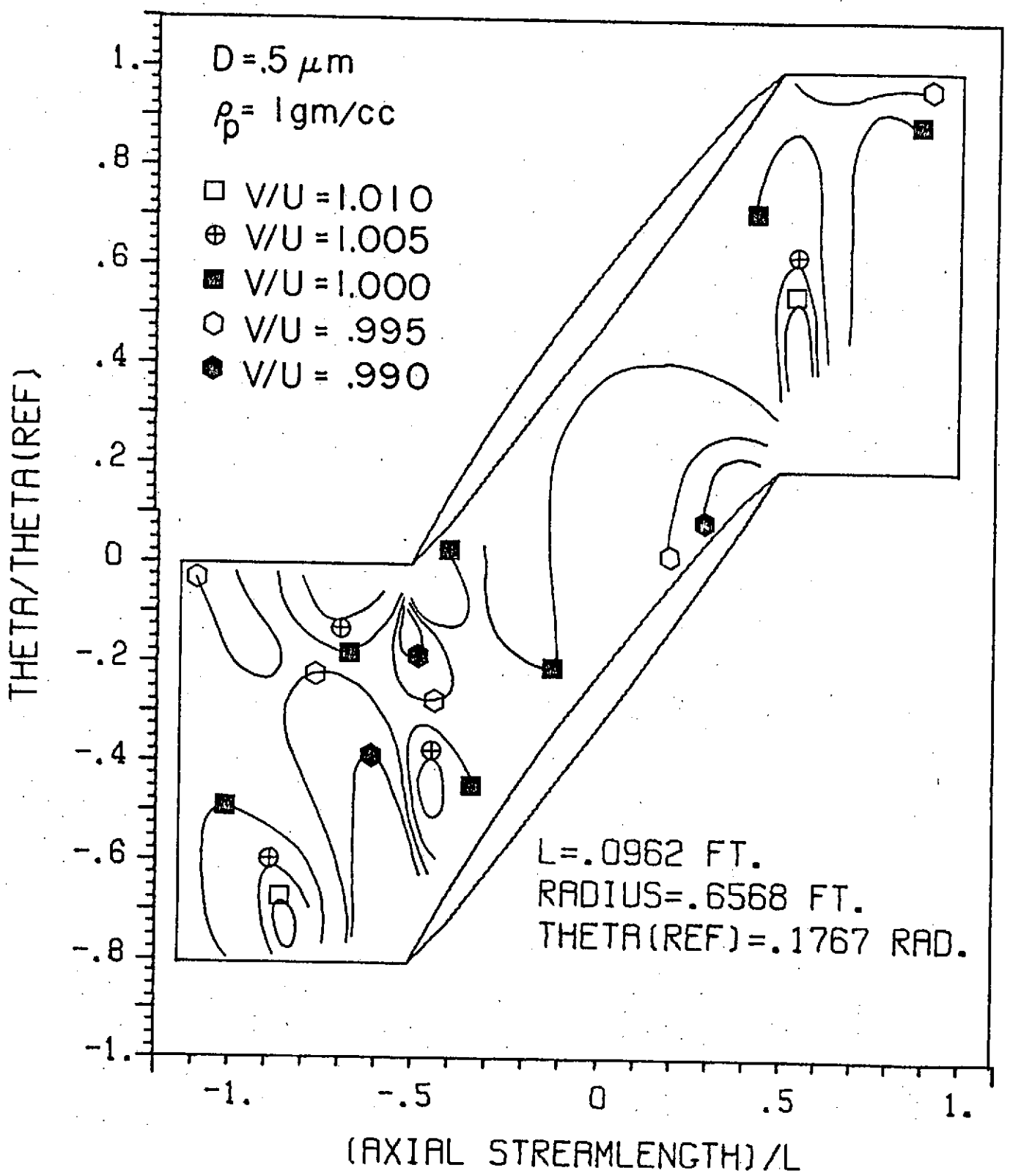

FIGURE 17A CONTOURS OF CONSTANT PARTICLE-TO-GAS VELOCITY RATIO, ρ_p = 1 gm/cc, r = .200 m

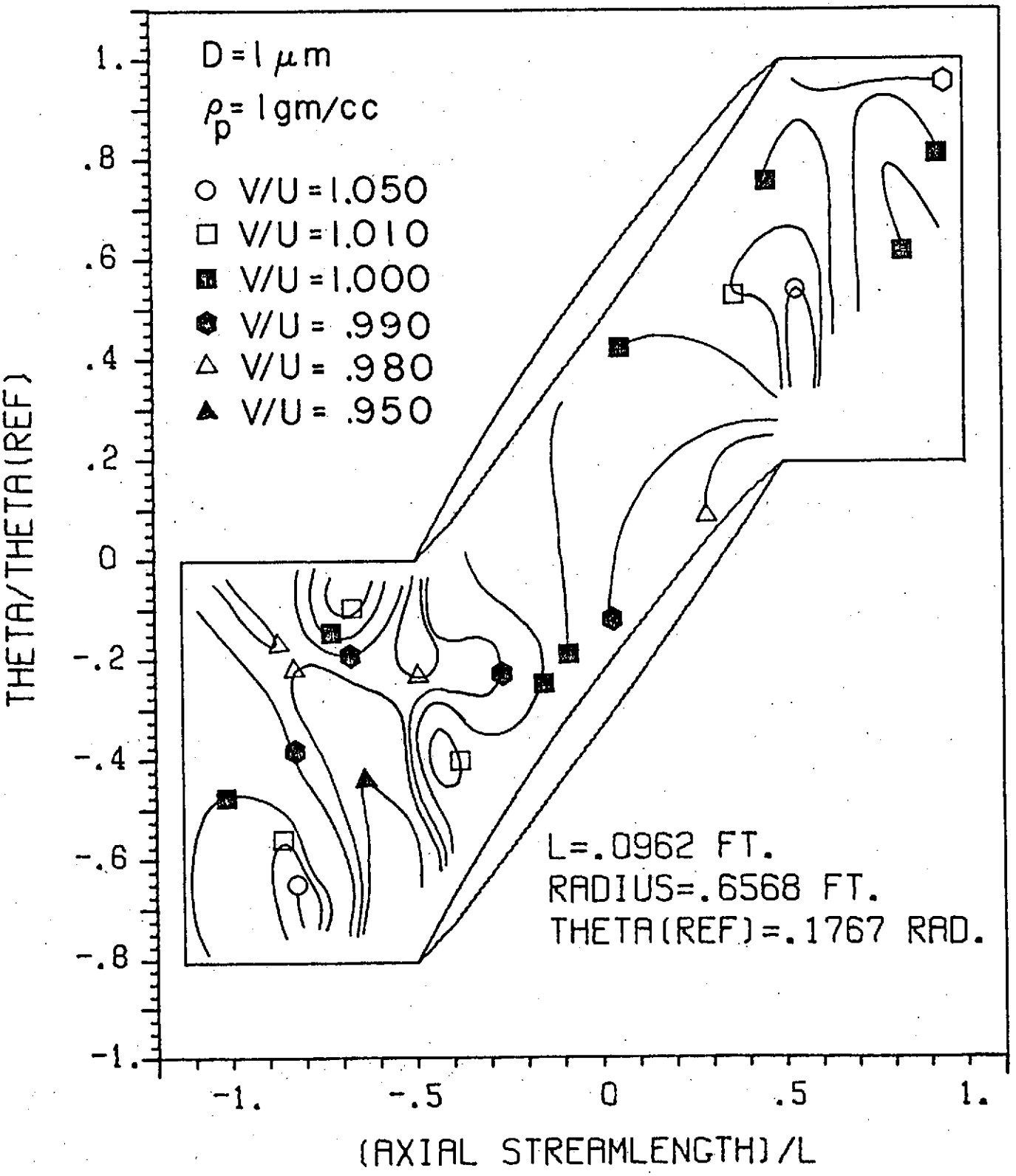

FIGURE 17B CONTOURS OF CONSTANT PARTICLE-TO-GAS VELOCITY RATIO, ρ_p = 1 gm/cc, r = .200 m

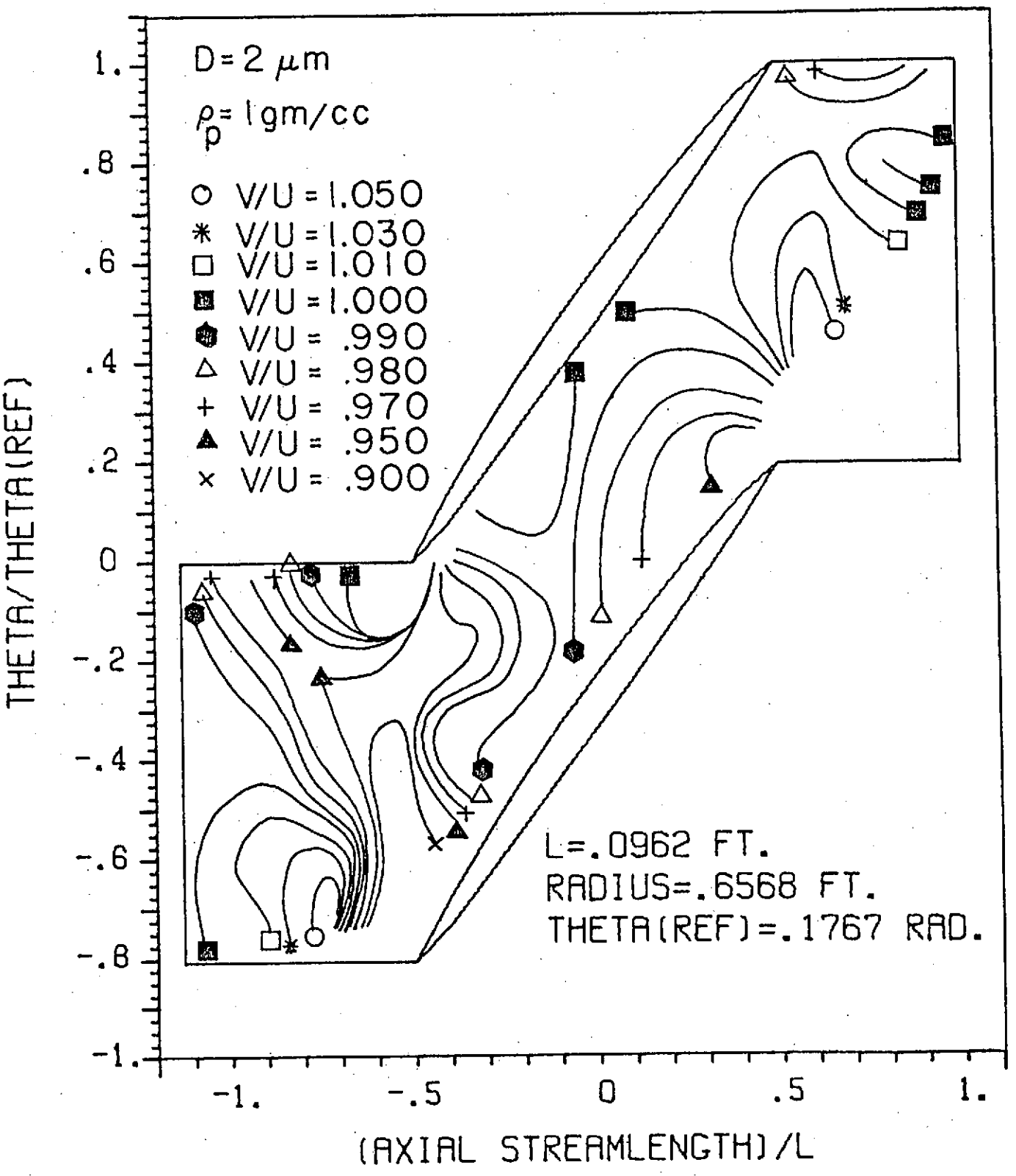

FIGURE 17c CONTOURS OF CONSTANT PARTICLE-TO-GAS VELOCITY RATIO, ρ_p = 1 gm/cc, r = .200 m

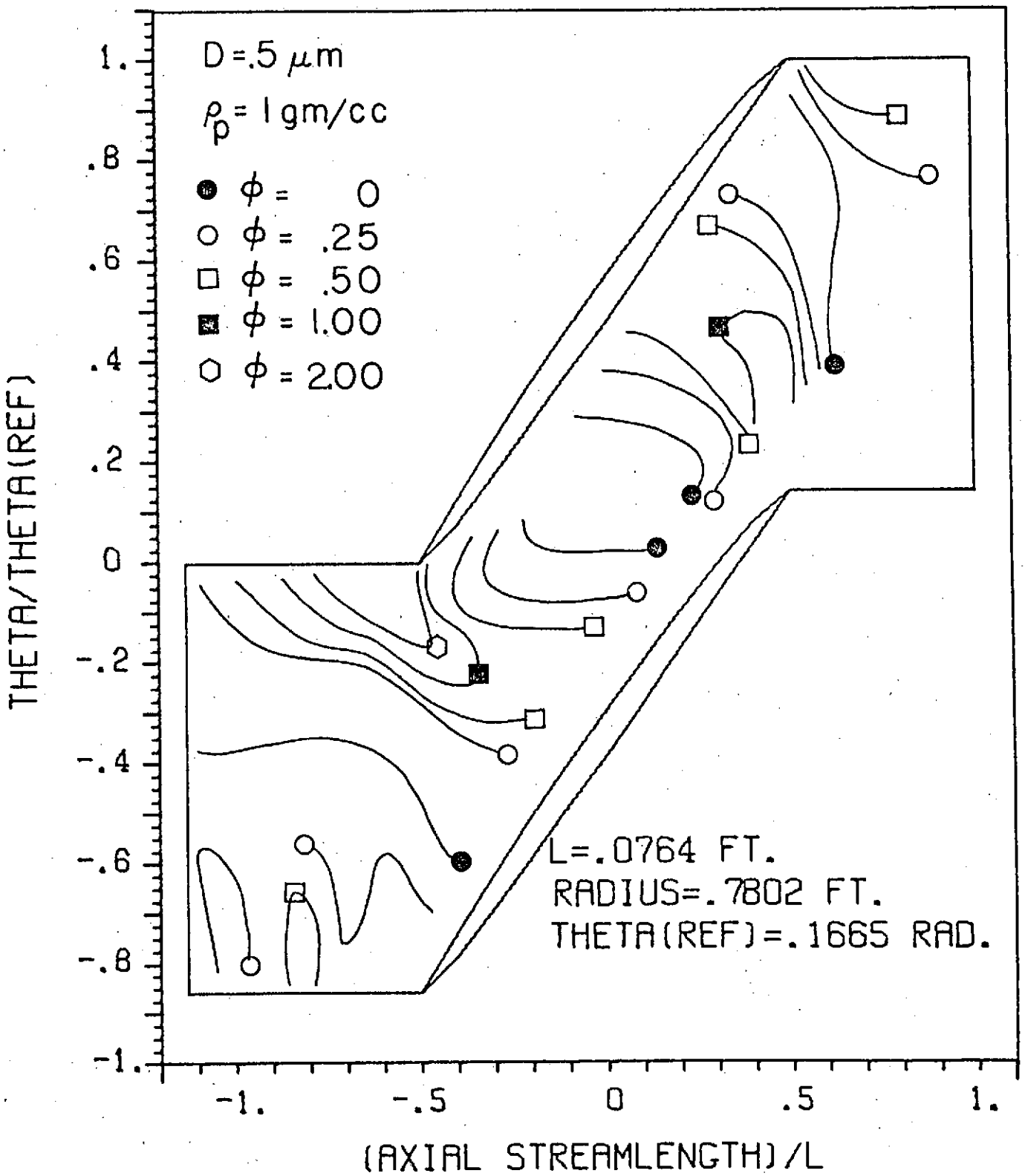

FIGURE 18A CONTOURS OF CONSTANT ANGULAR DEVIATION,
ρ_p = 1 gm/cc, r = .238 m

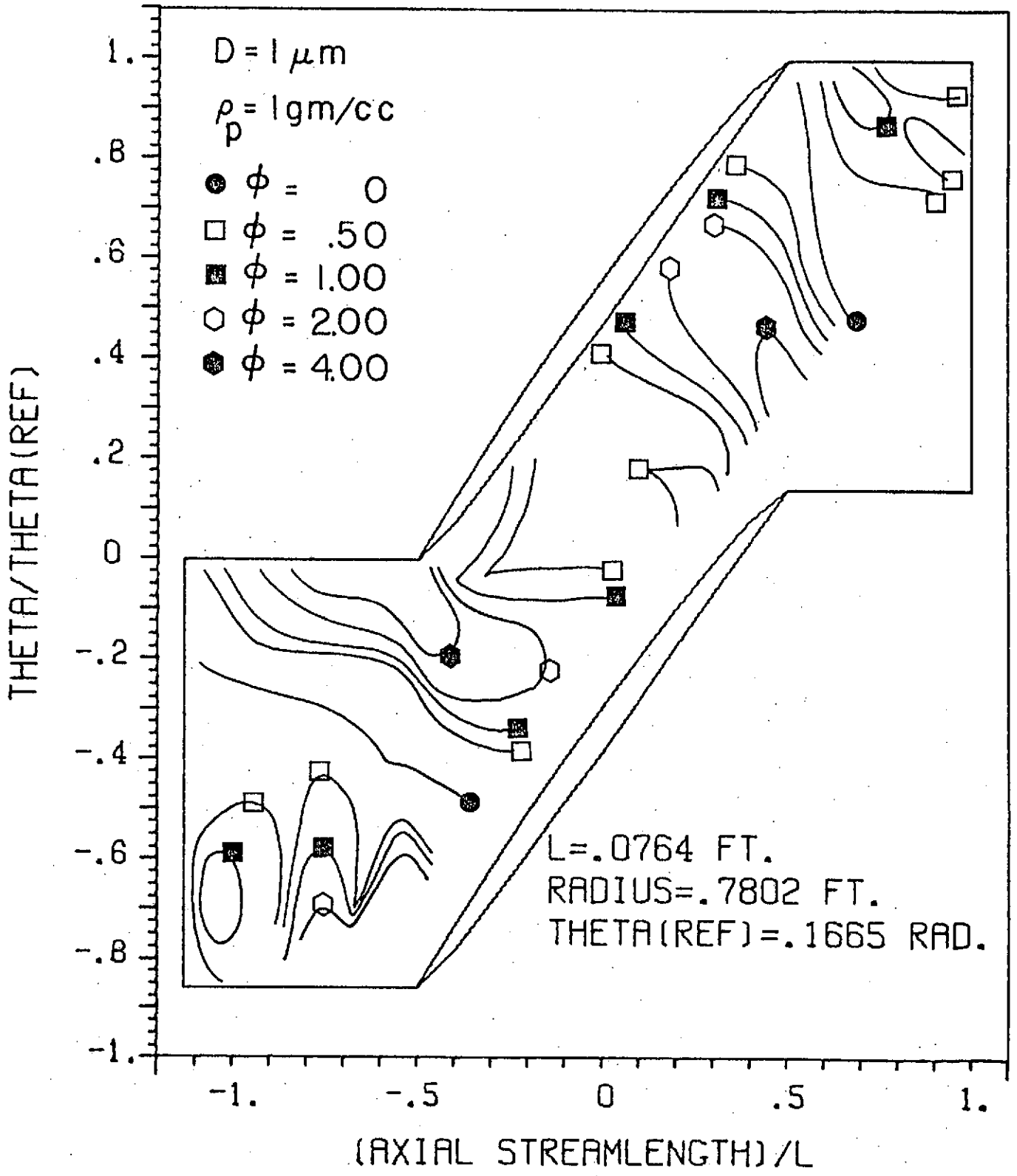

FIGURE 18B CONTOURS OF CONSTANT ANGULAR DEVIATION,
ρ_p = 1 gm/cc, r = .238 m

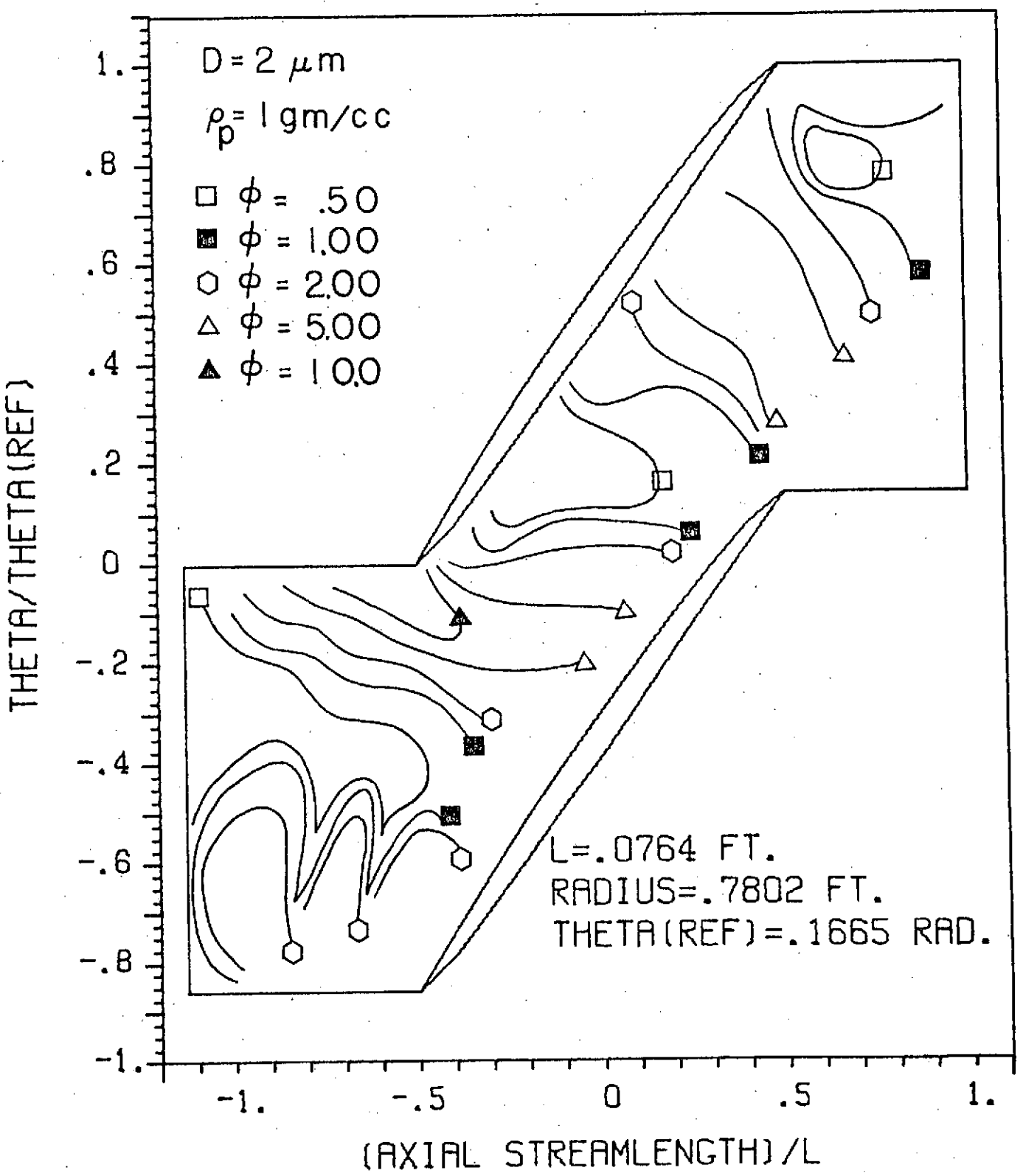

FIGURE 18c CONTOURS OF CONSTANT ANGULAR DEVIATION,
ρ_p = 1 gm/cc, r = .238 m

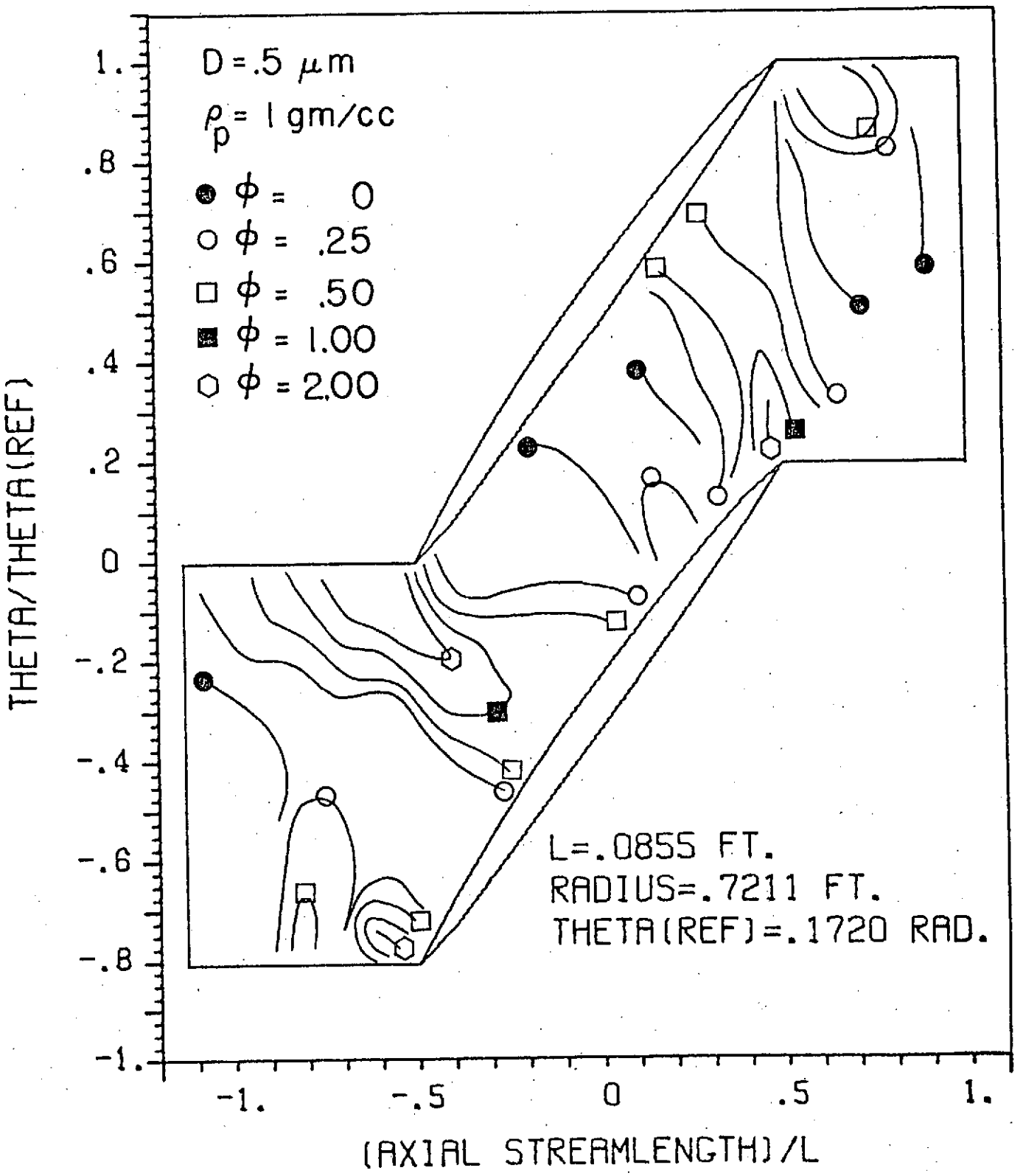

FIGURE 19A CONTOURS OF CONSTANT ANGULAR DEVIATION,
ρ_p = 1 gm/cc, r = .220 m

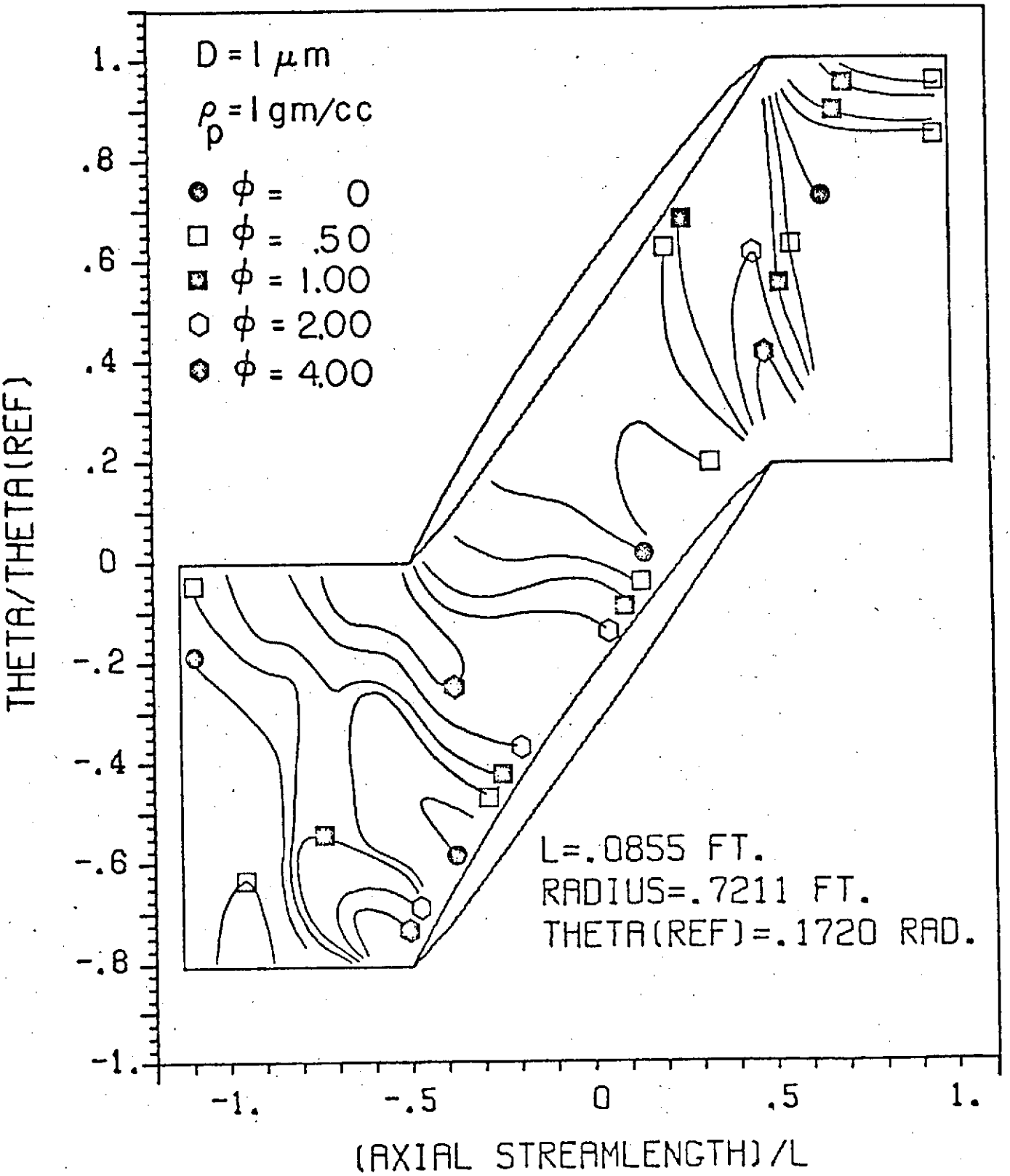

FIGURE 19B CONTOURS OF CONSTANT ANGULAR DEVIATION,
ρ_p = 1 gm/cc, r = .220 m

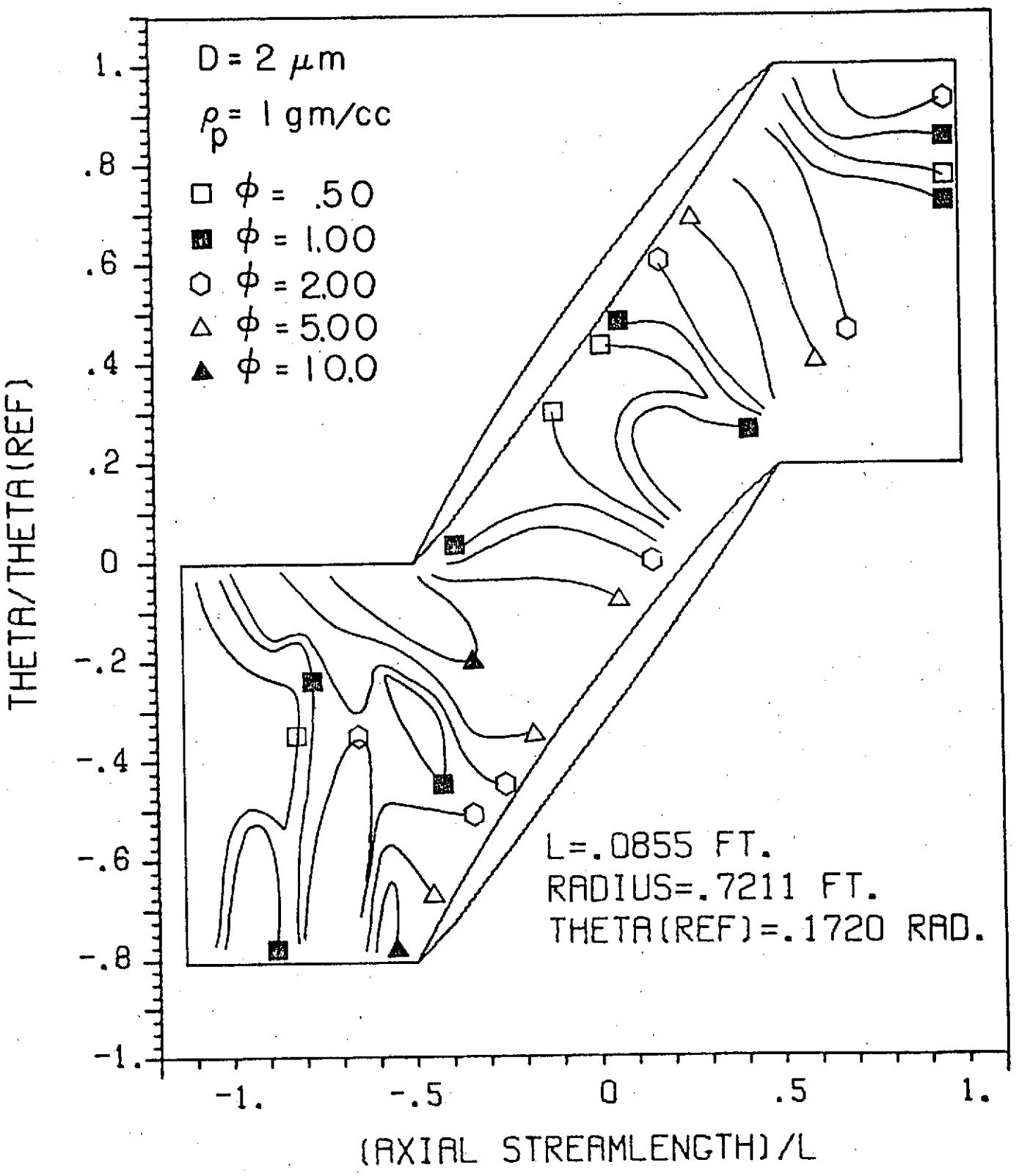

FIGURE 19c CONTOURS OF CONSTANT ANGULAR DEVIATION,
ρ_p = 1 gm/cc, r = .220 m

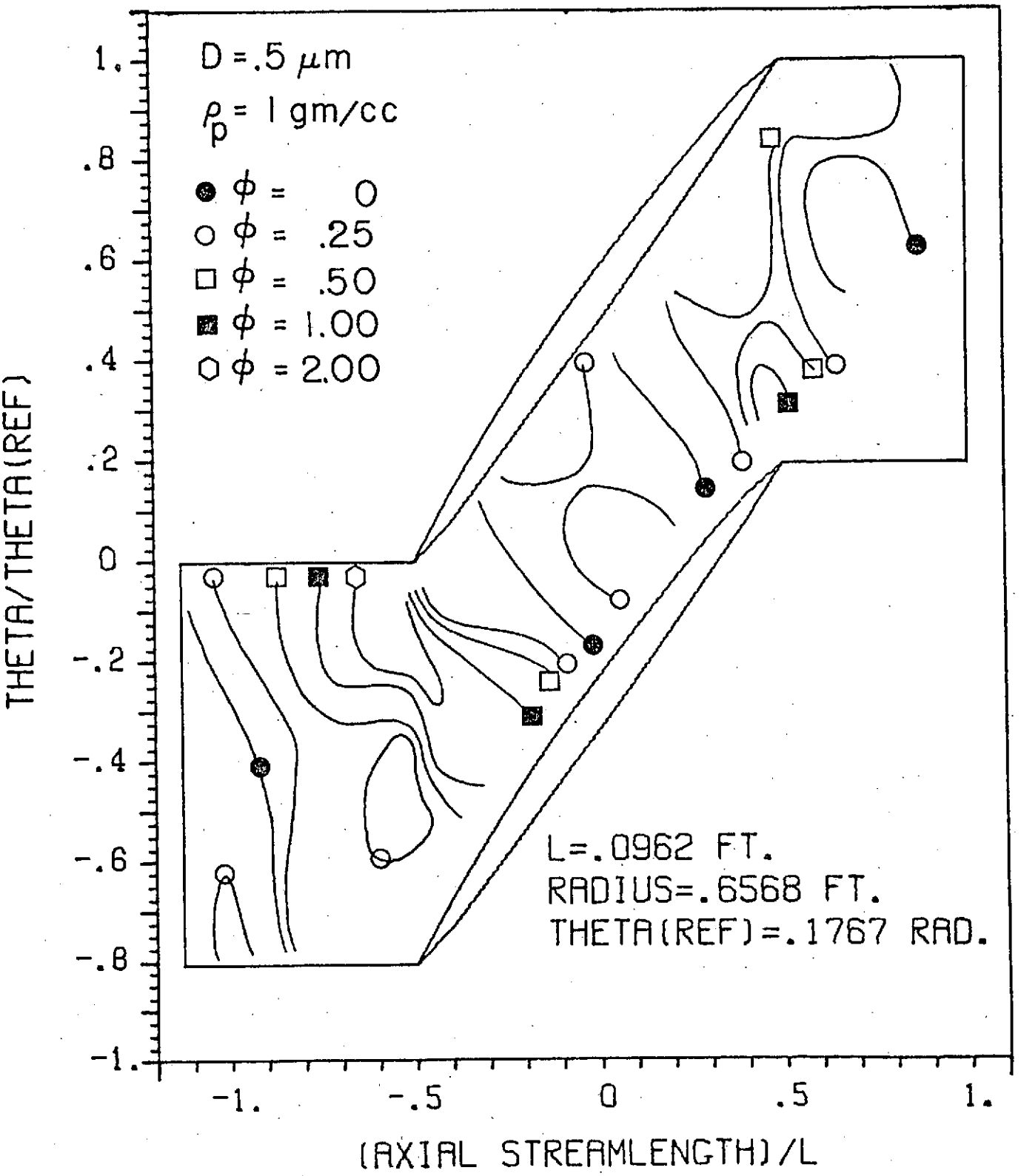

FIGURE 20A CONTOURS OF CONSTANT ANGULAR DEVIATION,
ρ_p = 1 gm/cc, r = .200 m

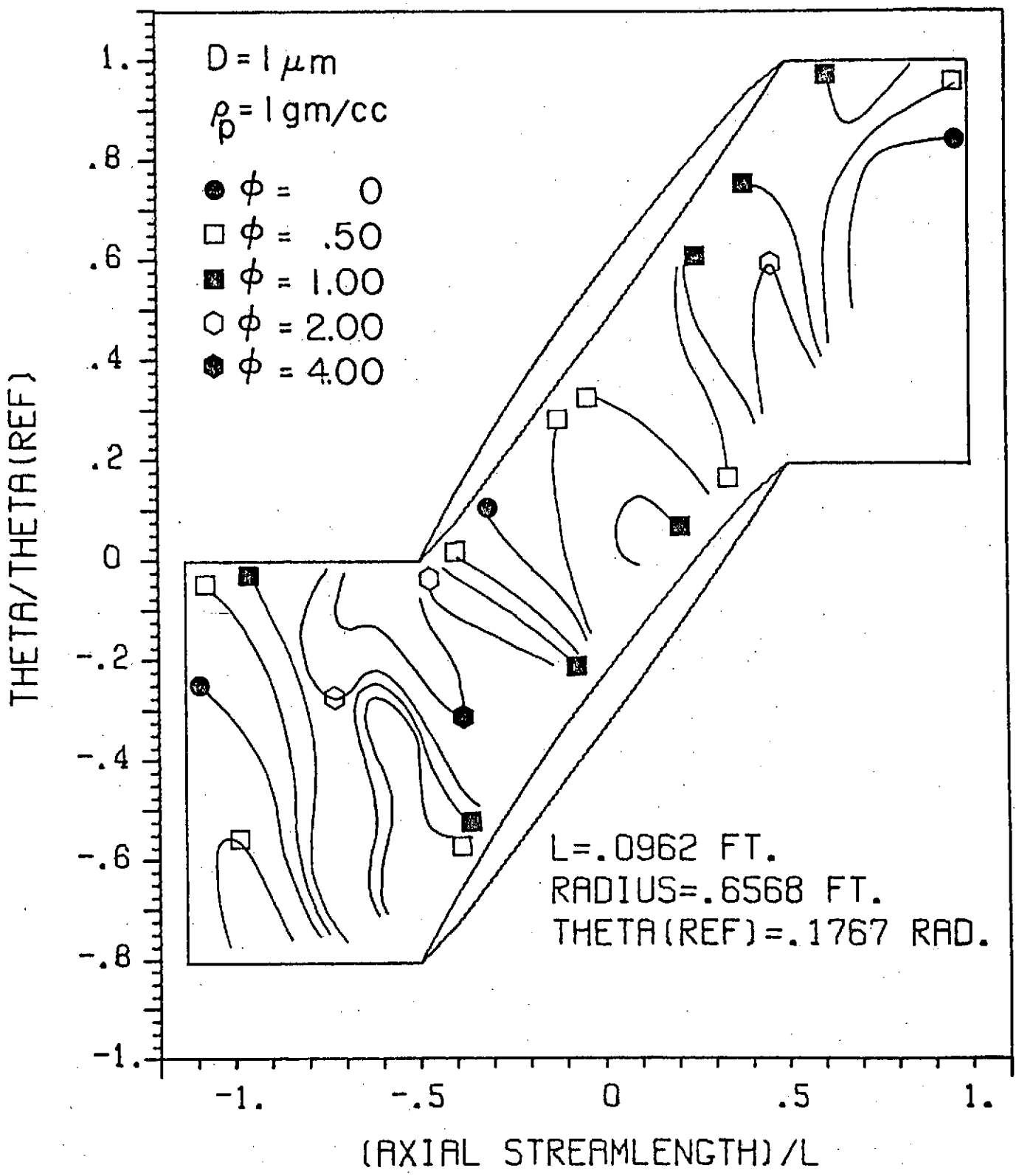

FIGURE 20B CONTOURS OF CONSTANT ANGULAR DEVIATION,
ρ_p = 1 gm/cc, r = .200 m

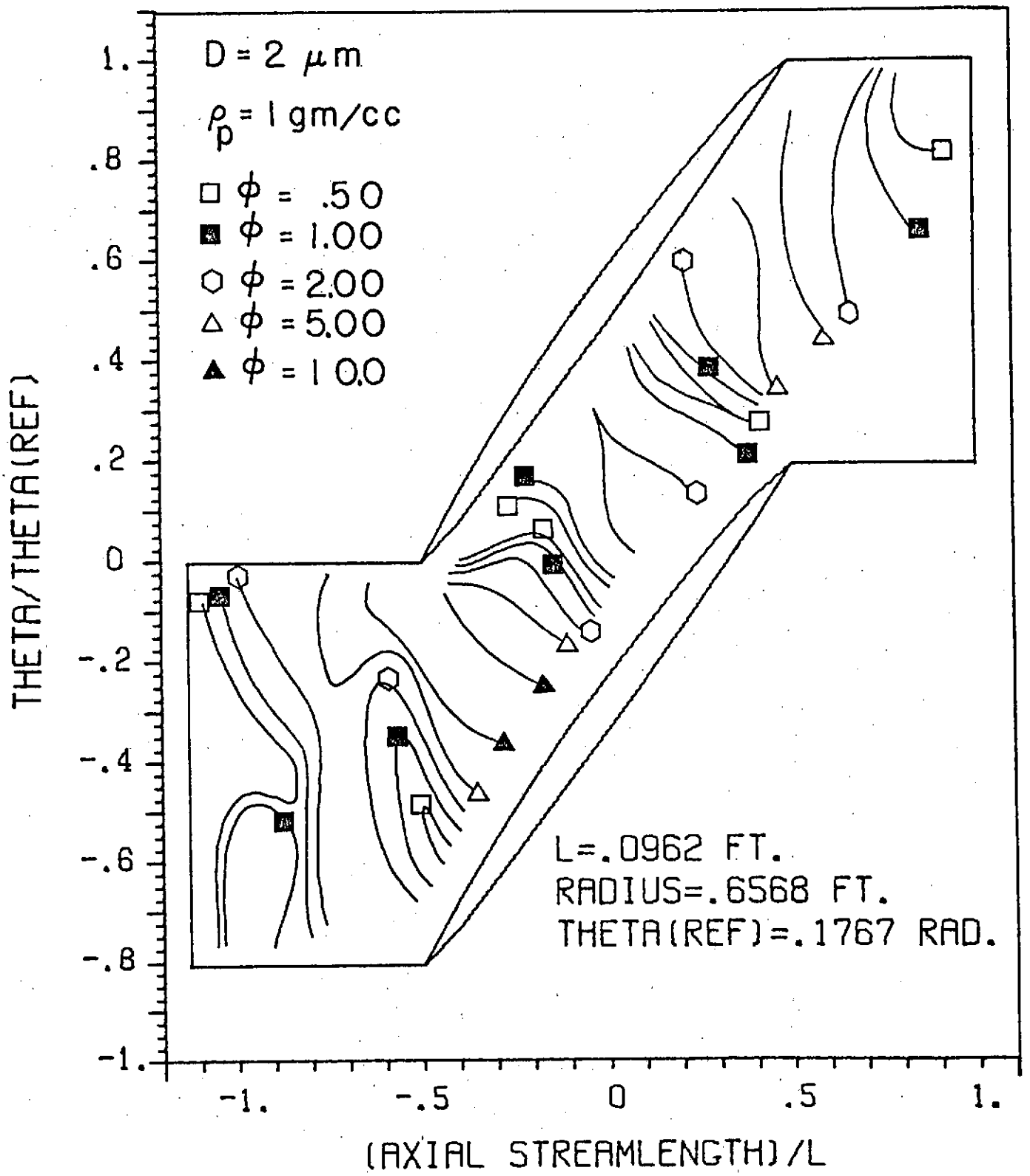

FIGURE 20c CONTOURS OF CONSTANT ANGULAR DEVIATION,
ρ_p = 1 gm/cc, r = .200 m

REPORT DISTRIBUTION LIST FOR NASA CR-134718

Dr. Richard G. Seasholtz (5)	NASA-Lewis Research Center Attn: R. G. Seasholtz (MS 77-1) 21000 Brookpark Road Cleveland, OH 44135
Mr. Melvin J. Hartmann (1)	NASA-Lewis Research Center Attn: M. J. Hartmann 21000 Brookpark Road Cleveland, OH 44135
Mr. Cavour H. Hauser (1)	NASA-Lewis Research Center Attn: C. H. Hauser 21000 Brookpark Road Cleveland, OH 44135
Dr. Theodore Katsanis (1)	NASA-Lewis Research Center Attn: T. Katsanis 21000 Brookpark Road Cleveland, OH 44135
Dr. William W. Hunter (1)	NASA-Langley Research Center Attn: W. W. Hunter Hampton, Virginia 23665
Mr. Richard Rivir (1)	Air Force Aero Propulsion Laboratory Air Force Systems Command Wright-Patterson AFB, OH 45433
Patent Counsel (1)	NASA-Lewis Research Center Attn: N. T. Musial (MS 500-113) 21000 Brookpark Road Cleveland, OH 44135
NASA Headquarters technical information abstracting and dissemination facility (40)	NASA Scientific and Technical Information Facility Attn: Acquisitions Branch P. O. Box 33 College Park, MD 20740
Lewis Library (2)	NASA-Lewis Research Center Attn: Library (MS 60-3) 21000 Brookpark Road Cleveland, OH 44135
Lewis Management Services Division (1)	NASA-Lewis Research Center Attn: Report Control Office (MS 5-5) 21000 Brookpark Road Cleveland, OH 44135